



UNIVERSITÀ  
DEGLI STUDI  
DI PADOVA

Università degli Studi di Padova

Dipartimento dei Beni Culturali: Archeologia,  
Storia dell'Arte, del Cinema e della Musica

Master Degree in  
ARCHAEOLOGICAL SCIENCES

Curriculum in  
APPLIED SCIENCES TO CULTURAL HERITAGE MATERIALS  
AND SITES

Characterization of mural paintings from Motza  
and Caesarea Maritima, Israel: Insights into  
techniques and materials

Supervisor:

Prof. Michele Secco

Co-supervisor:

Dr. Giulia Ricci

Candidate: Maniki Nelli-Spyridoula

Matricola: 2081184

Academic Year 2023/2024



## Acknowledgments

I would like to express my deepest appreciation to my supervisor professor Michele Secco for his assistance and precious support during the execution and writing of the thesis.

I am also thankful to my co-supervisor Dr. Giulia Ricci, who generously provided me with her guidance and knowledge throughout the analyses and writing of this project.

I would like to extend my sincere thanks to Dr. Yotam Asscher for his valuable advice.

Lastly, I am grateful for my family for supporting me during my studies.

## Ringraziamenti

Desidero esprimere il mio più profondo apprezzamento al mio relatore, il professor Michele Secco, per la sua assistenza e il suo prezioso supporto durante l'esecuzione e la stesura della tesi.

Sono anche grata alla mia correlatrice Dott. Giulia Ricci, che mi ha generosamente fornito la sua guida e le sue conoscenze durante le analisi e la stesura di questo progetto.

Vorrei estendere i miei sinceri ringraziamenti al Dott. Yotam Asscher per i suoi preziosi consigli.

Infine, sono grato alla mia famiglia per avermi sostenuto durante gli studi.

## List of contents

List of figures.....	5
List of tables.....	8
Abstract.....	9
Sommario.....	10
1. Introduction.....	11
2. Roman wall paintings.....	12
3. The archaeological site of Motza.....	14
4. The archaeological site of Caesarea.....	16
5. Materials and methods.....	18
5.1 Sample description.....	18
5.2 Sample preparation.....	21
5.3 Optical microscopy (PML).....	23
5.4 Micro-Raman spectroscopy.....	23
5.5 Scanning Electron Microscopy – Energy Dispersive Spectroscopy (SEM-EDS).....	24
5.6 X-ray diffraction (XRD) – X-ray powder diffraction (XRPD).....	25
6. Results and discussion.....	27
6.1 Optical microscopy (PLM).....	27
6.2 micro-Raman spectroscopy.....	34
6.3 Scanning Electron Microscopy – Energy-dispersive X-ray Spectroscopy (SEM-EDS).....	39
6.4 X-ray diffraction – X-ray powder diffraction (XRD-XRPD).....	48
7. Conclusions.....	54
8. Bibliography.....	55

## List of figures

- **Figure 1.** Aerial view from Google Maps showing the location of Motza, Israel.
- **Figure 2.** Excavation plan.
- **Figure 3.** Fresco fragments discovered under the floor.
- **Figure 4.** a) Ancient Caesarea and harbors, July 10, 1995 (North), b) Map of ancient Caesarea and key sites.
- **Figure 5.** The peristyle courtyard.
- **Figure 6.** Fresco fragments from the wall and ceilings.
- **Figure 7.** Samples of fragments placed in molds, before the pouring of resin, Department of Geosciences, Padova, Italy.
- **Figure 8.** Micro-Raman spectrometer, Department of Chemistry, Padova
- **Figure 9.** Quorum Q150R, Chemistry Department, Padova.
- **Figure 10.** a) Powder of 0.8g of sample, grinded using pestle and mortar, b) Sample fragments placed on metal disc, ready to be set in the diffractometer. Department of Geosciences, Padova.
- **Figure 11.** Sampled area of MF1ii cross section from MF1 fragment (a), microscope photos of the sample's stratigraphy (b,c).
- **Figure 12.** Sampled areas of MF5i (a(i),b,c,d) and MF5ii (a(ii),e,f,g), with microscope photos indicating each sample's stratigraphy.
- **Figure 13.** Sampled areas of MF9, with microscope photos indicating the sample's stratigraphy.
- **Figure 14.** Sampled areas of MF10i (a(i),b,c,d) and MF10ii (a(ii),e,f,g), with microscope photos of each sample.
- **Figure 15.** Sampled areas of MF14i (a(i)) and MF14ii (a(ii)), with microscope photos of each sample.
- **Figure 16.** Samples CF1(1), CF2(2), CF3(3) and CF4(4), with microscope photos of each sample (a,b,c,d).
- **Figure 17.** Sampled area of CF5i (a), with microscope photos of the sample (b,c,d).
- **Figure 18.** Samples from Motza showcasing their mortar's stratigraphy. MF13(a), MF10i(b), MF1ii(c), MF8(d), MF6(e), MF9i(f).
- **Figure 19.** Samples from Caesarea showcasing their mortar's stratigraphy. CF1(a), CF5i(b), CF2(c), CF5ii(d), CF4(e), CF6ii(f).
- **Figure 20.** Image of the area of MF1ii sample where the beam was directed (red circle in c), from the optical microscope (b) and Raman instrument (c).  $\mu$ -Raman spectrum of the yellow particle (a) showing typical goethite bands.
- **Figure 21.** a)  $\mu$ -Raman spectrum of the whiteish layer of MF2ii showing the characteristic quartz band, pictured in b) from the optical microscope. d)  $\mu$ -Raman spectrum of the yellow layer showing typical goethite bands, pictured in c) from the  $\mu$ -Raman instrument.
- **Figure 22.** a)  $\mu$ -Raman spectrum of the orange pigment lump shown in b) of the sample CF6ii from the optical microscope showing the characteristic band of quartz.
- **Figure 23.** a)  $\mu$ -Raman spectra of the blue lump of MF5i indicated in c) from the Raman instrument where the beam was directed. In b) a picture from the

optical microscope indicative of the region is shown. The typical bands of Egyptian blue are shown.

- **Figure 24.** a)  $\mu$ -Raman spectra of the red lump of pigment of MF6 indicated in c) from the Raman instrument where the beam was directed. In b) a picture from the optical microscope indicative of the region is shown. The typical bands of hematite are shown.
- **Figure 25.** a)  $\mu$ -Raman spectra of the red layer of MF10i indicated in c) from the Raman instrument where the beam was directed. In b) a picture from the optical microscope indicative of the region is shown. The typical bands of hematite and carbon black are shown.
- **Figure 26.** a)  $\mu$ -Raman spectra of the red layer of MF8 indicated in c) from the Raman instrument where the beam was directed. In b) a picture from the optical microscope indicative of the region is shown. The typical bands of litharge and carbon black are shown.
- **Figure 27.** a)  $\mu$ -Raman spectra of the black layer of MF3 with a microscope image of the sample MF3 indicating where the beam was directed (b). Characteristic bands of carbon black and calcite are shown.
- **Figure 28.** a)-b) EDS spectra of the first yellow and second red to black layer of the sample MF1ii. The spectra were obtained from the areas indicated in the SEM (in BSE) (c) and PLM (d) photos.
- **Figure 29.** a)EDS spectra of the green pictorial layer of sample MF7ii. b) SEM image in BSE of the analyzed area and an optical microscope image of the same area.
- **Figure 30.** a)EDS spectra of the green pictorial layer of sample MF9i. b) SEM image in BSE of the analyzed area and an optical microscope image of the same area.
- **Figure 31.** a)EDS spectra of the blue lump of pigment of sample MF5i. b) SEM image in BSE of the analyzed lump and an optical microscope image of the respective area.
- **Figure 32.** a)EDS spectra of the red pictorial layer of sample MF8. b) SEM image in BSE of the analyzed area and an optical microscope image of the same area.
- **Figure 33.** a)EDS spectra of the red pictorial layer of sample CF1. b) SEM image in BSE of the analyzed area and an optical microscope image of the same area.
- **Figure 34.** a)EDS spectra of the red overpainting layer of sample MF10i. b) SEM image in BSE of the analyzed area and an optical microscope image of the same area.
- **Figure 35.** a)EDS spectra of the black layer of sample MF3. b) SEM image in BSE of the analyzed area and an optical microscope image of the same area.
- **Figure 36.** a)SEM image in BSE and (b) EDS spectra of the plaster matrix of sample MF8. b) SEM image in BSE and EDS spectra (d) of the plaster of sample CF5i.
- **Figure 37.** EM images in BSE showcasing the layering of mortars in samples from Caesarea.
- **Figure 38.** XRD pattern of sample CF1.

- **Figure 39.** XRD pattern of sample MF1.
- **Figure 40.** XRD pattern of sample MF3.
- **Figure 41.** XRD pattern of sample MF4.
- **Figure 42.** XRD pattern of sample MF9.
- **Figure 43.** XRD pattern of sample MF10.
- **Figure 44.** XRD pattern of sample MF15.
- **Figure 45.** XRPD pattern of sample CF6-M.
- **Figure 46.** XRPD pattern of sample MF8-M.
- **Figure 47.** XRPD pattern of sample MF15-M.

## List of tables

- **Table 1.** Sample groups, photos and notes.
- **Table 2.** Complete list of cross section samples.
- **Table 3.** Samples, number of layers and painting techniques of all the analyzed samples.
- **Table 4.** Sample names and phases detected with the XRD/XRPD.



## Abstract

This thesis presents a detailed investigation of the mural paintings excavated from the archaeological sites of Motza and Caesarea Maritima, Israel. The primary objective is to analyze fragments of wall paintings to discern the painting techniques employed, identify the pigments used, and determine the composition of the mortars.

To achieve these aims, cross-sections were prepared from representative parts of each fragment, allowing for a thorough microscopic analysis of the stratigraphy, pigment distribution, and mortar composition. Optical microscopy provided initial insights, revealing the layering, pigment lumps, and characteristics of the mortars.

Subsequently, micro-Raman spectroscopy was utilized to define the micro-mineralogical composition of both pigments and mortars. This technique offered precise identification on the composition of most of the pigments, including yellow, black, and red. Nevertheless, it yielded limited data for colors such as green and blue, characterized by weak Raman signals. In such cases, and for further confirmation and detailed analysis of the already determined compositional and textural features, scanning electron microscopy coupled with energy-dispersive X-ray spectroscopy (SEM-EDS) was applied, providing comprehensive microstructural and microchemical information on the analyzed samples.

Additionally, X-ray diffraction (XRD) was utilized to examine the mineralogical composition of the painted surfaces. This approach provided valuable insights into the mineral phases present within the paint layers, aiding in understanding the source of raw materials and potential alteration processes over time. Moreover, XRD analysis of powder fractions from the mortar components elucidated their mineralogical composition, offering further understanding of the geological sources and production techniques utilized in mortars' preparation.

Through this multidisciplinary approach, this study provided significant insights into artistic techniques, material composition, and construction practices employed in ancient sites of Motza and Caesarea Maritima. The findings enrich our understanding of the cultural heritage of the region, shedding light on the artistic practices and technological knowledge of past civilizations.

## Sommario

Questa tesi presenta un'indagine dettagliata delle pitture murali scavate nei siti archeologici di Motza e Cesarea Maritima, in Israele. L'obiettivo principale è quello di analizzare i frammenti di pitture murali per discernere le tecniche pittoriche impiegate, identificare i pigmenti utilizzati e determinare la composizione delle malte.

Per raggiungere questi obiettivi, sono state preparate sezioni trasversali da frammenti rappresentativi di ciascun campione, consentendo un'analisi microscopica approfondita della stratigrafia, della distribuzione dei pigmenti e della composizione delle malte. La microscopia ottica ha fornito le prime indicazioni, rivelando la stratificazione, la presenza di grumi di pigmento e le caratteristiche morfologiche delle malte.

Successivamente, è stata utilizzata la spettroscopia micro-Raman per definire la composizione micro-mineralogica dei pigmenti e delle malte. Questa tecnica ha permesso di identificare con precisione la composizione della maggior parte dei pigmenti, tra cui il giallo, il nero e il rosso. Tuttavia, ha fornito dati limitati per colori come il verde e il blu, caratterizzati da deboli segnali Raman. In questi casi, per un'ulteriore conferma e analisi dettagliata, è stata applicata la microscopia elettronica a scansione accoppiata alla spettroscopia a raggi X a dispersione di energia (SEM-EDS), che ha fornito informazioni microstrutturali e microchimiche complete sui campioni analizzati.

Inoltre, è stata utilizzata la diffrazione di raggi X (XRD) per esaminare la composizione mineralogica delle superfici dipinte. Questo approccio ha fornito preziose indicazioni sulle fasi minerali presenti negli strati pittorici, aiutando a comprendere la fonte delle materie prime e i potenziali processi di alterazione nel tempo. Inoltre, l'analisi XRD polveri delle malte ha chiarito la loro composizione mineralogica, offrendo un'ulteriore comprensione delle fonti geologiche e delle tecniche di produzione utilizzate nella preparazione delle malte.

Grazie a questo approccio multidisciplinare, il presente studio ha fornito importanti indicazioni sulle tecniche artistiche, sulla composizione dei materiali e sulle pratiche costruttive utilizzate negli antichi siti di Motza e Caesarea Maritima. I risultati arricchiscono la nostra comprensione del patrimonio culturale della regione, facendo luce sulle pratiche artistiche e sulle conoscenze tecnologiche delle civiltà del passato.

## 1. Introduction

The study of Roman wall paintings holds significant value as it offers crucial insights into their manufacturing techniques, artistic materials employed, historical modifications, and facilitates appropriate conservation and restoration efforts. Research on Roman wall paintings, conducted across multiple sites in Italy, France, England, Spain, Switzerland, and Greece, primarily focuses on identifying pigments and binding agents (Piovesan *et al.*, 2011; Corso *et al.*, 2012) while some studies delve into examining painting methods and preparatory mortar layers (Piovesan *et al.*, 2011; Gutman *et al.*, 2016).

The aim of this work is to analyze the fragments of wall paintings from the archaeological sites of Motza and Caesarea in order to identify the painting techniques and pigments used and determine the composition of the mortar layers.

Motza, located in the vicinity of modern-day Jerusalem, emerges as an ideal site for the study of provincial Roman art in the Eastern Mediterranean. The discovery of wall paintings within the domestic spaces of Motza sheds light on the aesthetic tastes and cultural practices of its inhabitants during the Roman period. As a rural settlement situated along major trade routes, Motza offers a glimpse into the integration of local artistic traditions with broader Mediterranean influences, highlighting the adaptability and hybridity of Roman visual culture beyond urban centers. However, prior to the recent extensive excavations carried out at Motza between 2017 and 2019, scant information was available regarding the Roman settlement. Despite archaeological discoveries unearthed through limited-scale excavations and chance findings at the site, crucial details such as its chronology, constituent elements, or the demographics of its inhabitants remained largely elusive (Bar-Nathan, Di Segni and Taxel, 2020).

Conversely, the coastal city of Caesarea stands as a testament to the grandeur and cosmopolitanism of Roman urban life in the Levant. Established by Herod the Great, Caesarea flourished as a center of commerce, culture, and political power under Roman rule. The opulent villas and public edifices adorned with elaborate wall paintings attest to the city's status as a hub of artistic patronage and cultural exchange.

The subsequent chapters of this thesis will be dedicated to an examination of the archaeological sites of Motza and Caesarea, while then focusing on the preparation, analysis, and interpretation of fragments of wall paintings recovered from these locations. Employing a multidisciplinary approach, this study used Optical Microscopy, Micro-Raman Spectroscopy, Scanning Electron Microscopy (SEM), and X-Ray Diffraction (XRD) techniques to scrutinize the chemical and physical composition of both painting layers and mortars, focusing also on the identification of the employed painting techniques.

## 2. Roman wall paintings

It is known by references in surviving literatures that the Romans possessed a profound appreciation for the arts (Hallett, 2015). Contemporary scholarly discourse surrounding Roman paintings largely centers on the writings of prominent authors, notably the historian Pliny and the architect Vitruvius (Siddall, 2006). These esteemed figures serve as reliable sources with regard to the diversity of artists' color palettes. While Roman artists utilize the conventional color palette, detailed analyses have unveiled the emergence of distinct local and regional palettes. During the period that encompassed the zenith of Roman interior decoration, spanning from the 1st century BC to the 1st century AD, Vitruvius (Vitruvius, 1999) and Pliny (Pliny, 1952) produced writings that have come to epitomize Roman painted art.

Roman painted art is predominantly represented by wall paintings, primarily due to their higher likelihood of preservation in the archaeological record compared to portable panel paintings. The popularity of them was far from restricted to the reception rooms of the large homes of the wealthy Roman citizens but instead were found in the vast majority of rooms. These painted interiors were not confined to any particular social stratum but were rather a common feature in houses owned by individuals across the societal spectrum.

For wall paintings, there was the need of a smooth, flat and white ground layer (Piovesan *et al.*, 2012). Roman wall paintings were created using two techniques: *secco* on dry lime plaster or the *fresco* technique. The plaster layers supporting these paintings were constructed from multiple layers of lime plaster, while the uppermost layer contained a lime binder and a fine aggregate of crushed marble. According to Vitruvius, up to nine layers of plaster were supposed to be applied before painting. However, adherence to these rules decreased over time due to space limitations resulting from multiple redecoration schemes. As a result, the complexity of supports diminished over time. The range of support thickness varied significantly, spanning from approximately 10 centimeters thick with up to seven layers of plaster, to as thin as 2 millimeters of marmorino directly applied onto the rough wall. Greater care was taken when paintings were intended for exterior walls or damp areas, where crushed pot sherds were added to the lower coats, the fine-grained ones called *arricio* and the medium-fine ones *intonaco*. This addition reacted with slaked lime to create hydraulic cements that were not only waterproof but also capable of setting in a wet environment.

Lime plaster primarily consists of calcium carbonate along with sand and/or crushed pottery as aggregate. In the fresco technique, also known as *buon fresco*, calcium hydroxide is used in the lime wash as a binder for pigments, which, upon curing, transforms into calcium carbonate. The presence of calcium carbonate in many analyses can be attributed to the medium or contamination from the supports, although there are instances where it is intentionally added or even serves as the primary constituent of the pigment, particularly in the case of white pigments. These components create a stable, white background on which the paintings are executed. In addition, the practice of using undercoats to enhance the final color, as described by Pliny for use with reds, is widespread and not limited to bright pigment shades.

When it comes to the pigments use, we can create a short list of them based on the colors identified in wall paintings by various analyses utilizing either spectroscopic techniques or direct chemical analyses, and those recommended by Pliny and Vitruvius. Pliny categorizes pigments into two groups: the extravagant "florid" pigments, consisting of rare and costly materials, and the more commonplace pigments termed "austere" or subdued (Pliny, 1952). The florid pigments, which Pliny mentions as vermillion, azurite, malachite, and indigo, were procured and funded by the patron at their own expense. On the other hand, the remaining austere pigments were provided by the artist as part of the commission cost, including ochres, green earth, chalks, and Egyptian blue. These pigments encompass both natural and synthetic varieties.

Starting with the red pigments, the predominant ones were derived from red ochres, with hematite as the primary coloring component. Cinnabar was detected in a few paintings, often mixed with hematite, while organic reds from madder were also identified in Pompeii and red lead was reported only by Augusti in previous studies. Blue pigments were primarily derived from Egyptian Blue, a calcium copper silicate produced through calcination. This pigment was widely used in Roman wall paintings, with lapis lazuli (ultramarine) and indigo mentioned as potential alternatives, with the use of ultramarine being uncertain before the 6th Century AD. For purple colors, Tyrian Purple, derived from shellfish, was listed by Roman authors but was not conclusively detected in wall paintings, likely due to its high value. Reddish purples were created through various methods, including heat treatment of hematite and mixing hematite with Egyptian Blue or organic dyes like madder and indigo. Green pigments were derived from malachite, green earth, verdigris, and other copper corrosion products. Malachite was detected in Pompeii, and green earth was commonly used, sometimes mixed with Egyptian Blue. Yellow pigments were sourced from yellow ochre (goethite), orpiment (arsenic sulfide), and massicot (lead oxide). Yellow ochre was identified in all paintings, while orpiment's presence is inconclusive and massicot was detected in some instances. White pigments were diverse, including various forms of calcium carbonate, possibly derived from crushed limestone, chalk, mollusc shells, or bird eggs. Mg carbonate (dolomite) and aragonite were also reported. Diatomite, composed of microscopic diatom frustules, was used as a substrate for organic dyes in Pompeii, while lead carbonate (lead white) was identified in Pompeii as well. Black pigments mainly consisted of carbon-based blacks, although the source of carbon was often unclear. Coal and bone-black were reported in a villa near Vicenza, and charcoal was found in some instances. The only mineral black identified was manganese oxide pyrolusite, detected in Nea Paphos on Cyprus.

### 3. The archaeological site of Motza

Motza is a neighborhood on the western edge of West Jerusalem, located in the Judean Hills, 600 meters above sea level (**Fig. 1**). Numerous surveys and excavations have been conducted in the area over time, notably by the Israel Antiquities Authority as part of salvage excavations preceding the construction of a new road to Jerusalem (Greenhut *et al.*, 2009). These excavations occurred in 1993, 2002, 2003 and in 2012–2013. The site, identified as an archaeological tell, exhibited evidence of intermittent occupation from the Pre-Pottery Neolithic period (8th-7th millennia BCE) to the 20th century (Ad, Bar-Nathan and Taxel, 2022). Notably, extensive findings dating to the Iron Age II (10th to 6th centuries BCE) were unearthed during these excavations, confirming the site's association with biblical *Mozah*, mentioned in the Book of Joshua as a city within the territory of the tribe of Benjamin. The excavations revealed also continuous settlement during the Iron Age II period (Kisilevitz and Lipschits, 2019).

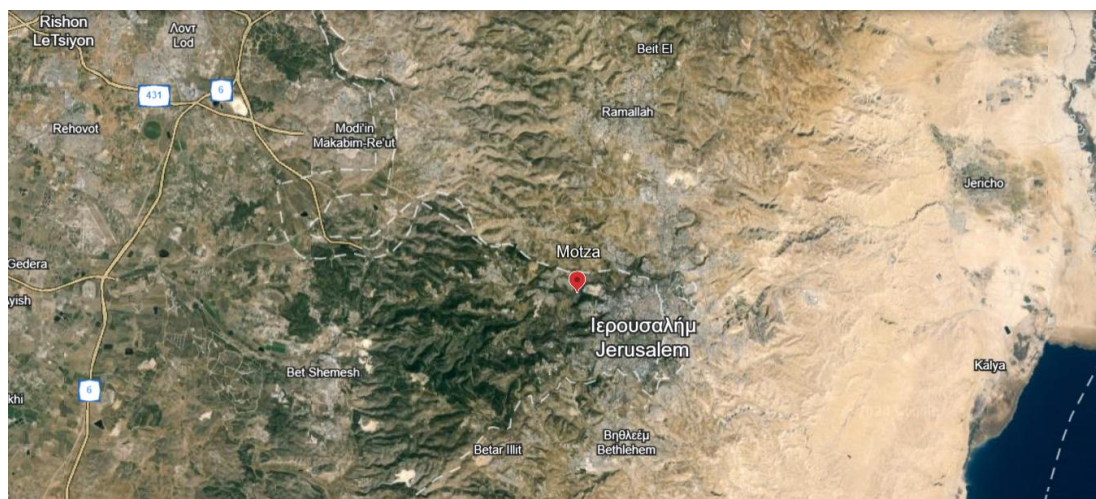


**Figure 1.** Aerial view from Google Maps showing the location of Motza, Israel.

In addition, there was the revelation of the remains of a large, planned Roman and Byzantine periods settlement. The most recent excavations (bar-nathan, Di Segni and Taxel, 2020), dated between 2015 and 2020, bolster the assertion that the site corresponds to the Roman veterans' settlement established by Vespasian after the Great Jewish Revolt (70 AD), as was expected according to Josephus (Josephus, 1928). The site is positioned approximately 5km west of present-day Jerusalem and about 0.5km from Tel Motza. It sits on a sloping spur facing west, close to the convergence of Nahal Soreq and Nahal Arza, with a small spring flowing from the west towards it. Despite limited historical records regarding this settlement, the aforementioned excavations yield significant insights into its architectural features, population, and material artifacts, shedding light on its characteristics and significance.

Specifically, excavations in areas B1 and D9 (**Fig. 2**) exposed remains of a settlement from the Middle Roman, Late Roman and Byzantine periods, revealing over eight dunams of the Roman settlement, whose first phase of existence is dated between the 1st and the 2nd century AD. The excavations from 2019 to 2020, have also provided valuable information about the extent of the settlement. In particular, the western and eastern boundaries were identified during these excavations, suggesting that the

settlement spanned approximately 170 meters in an east-west direction. Although the southern boundary was determined in earlier excavations conducted between 2018 and 2019, the northern limits remain unknown. However, it is estimated that the settlement covered over 16 dunams, potentially reaching between 20 to 25 dunams in size. Archaeological remains from this period, particularly in the southern and western areas, include field walls, tombs, and plastered installations.



**Figure 2.** Excavation plan.

The fragments that have been analyzed in the later parts of this work were found in two different fills in the site of Motza, specifically under the floors of the Late Roman period (70 – 130 AD) in the eastern part of the northern segments and the courtyard, of a peristyle structure in area G1 (**Fig. 3**). A large prosperous residence was designed as the aforementioned square peristyle structure was uncovered northwest of the street during the second period of excavations, constituting nearly a third of the settlement’s excavated area. Constructed during the Middle Roman period, this structure remained in use until the 4th century AD, with two distinct Middle Roman phases identified. In the center of the structure a courtyard was also uncovered, surrounded on all four sides by a portico.



**Figure 3.** Fresco fragments discovered under the floor.

Those fragments of fresco and stucco that embellished the walls of the first and second phases mirror the opulent nature of the building. They also provide evidence of sumptuous structures with rooms whose walls were decorated with frescos.

#### 4. The archaeological site of Caesarea

Caesarea Maritima, commonly known as Caesarea Palaestinae from ancient texts, was built by the Jewish king Herod the Great 22-10/9 B.C.E during a period of intense construction activity that defined the third decade of its governance (Rabbān and Holum, 1996; Fuhrmann-Naaman, 2017). It was located on the Mediterranean coast in the northern part of the Sharon plain and featured a significant artificial harbor (**Fig. 4**)

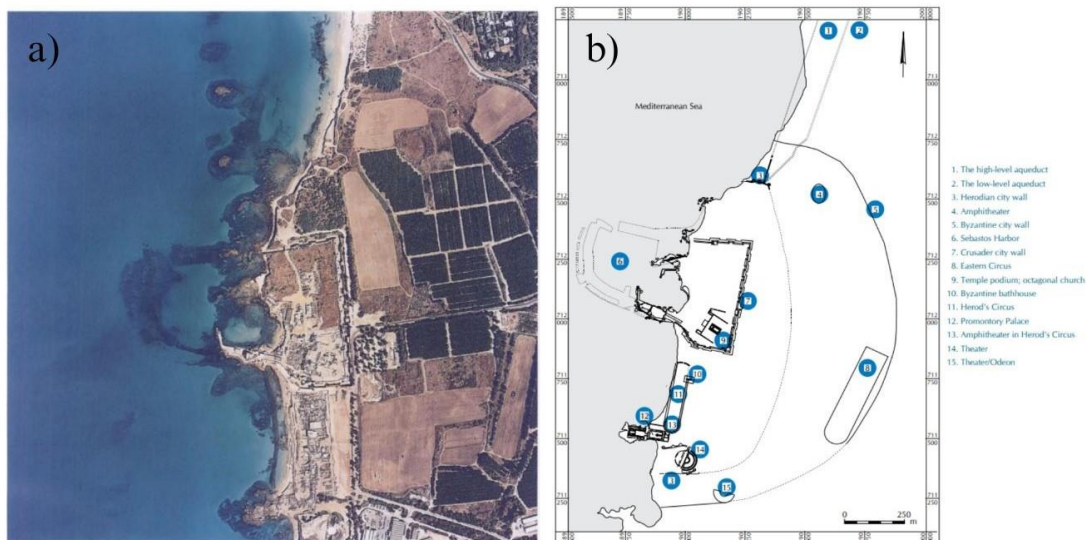


**Figure 4.** a) Ancient Caesarea and harbors, July 10, 1995 (North), b) Map of ancient Caesarea and key sites.

In the western part of the Sharon plain, there are three *kurkar* ridges (local calcareous-cemented aeolianite sandstone (Vola *et al.*, 2011)), running parallel to the coast. These ridges enclose shallow troughs between them. The ridge closest to the sea has been partially eroded by wave action. In the northern section of the Sharon coastline, some



islands and peninsulas from this westernmost ridge still exist. These geographical features provided a relatively convenient anchorage for Straton's Tower, the precursor to Caesarea. During Herod's time, some of these islands were incorporated into the construction of the artificial harbor.

The climate around Caesarea follows the typical Mediterranean pattern, characterized by hot and humid summers, as well as moderate and rainy winters, with transitional seasons in between. The region receives an average annual rainfall of about 550 mm. Freshwater springs are present near the troughs and the beach, owing to the proximity of the aquifer to the surface. These springs were historically utilized. The soil in the area is sandy, resulting from the penetration of dunes formed by Nahal Hadera through the *kurkar* ridges.

Since the 1950s and 1960s, extensive archaeological excavations have been ongoing, with volunteers laboring under the guidance of archaeologists. The primary contributors to these excavations are the United States and Israel, who continue to spearhead much of the archaeological research to the present day (Holum, Stabler and Reinhardt, 2008).

One of the wealthy Roman houses, from which the samples presented later on this work originate, was excavated in 1992-1996 (Gendelman and Gersht, 1997). This is the *House of Dioscuri* (no. 10 in **Fig.4,b**), the only one among the Roman houses that was excavated on such an extensive scale. Its construction took place during the initial decades of the 1st century AD and it was situated as the second building in the western row of structures south of the temple platform dedicated to Augustus and the goddess Roma, positioned near the harbor. Prior to its erection, no remnants were discovered in the vicinity, except for those related to the Straton Tower cemetery, which represents the earlier Hellenistic settlement predating Caesarea. The house was bounded to the north, south, and east by streets, while its western side was adjacent to a promenade that ran alongside the rear of Herod's Circus (no. 8 in **Fig. 4,b**). The house, measuring 90 meters in length and 37 meters in width (excluding the shops), extended across an area of three dunams. It comprised three levels accessible via two to three sets of stairs. The southern level was constructed around an atrium, while the intermediate level surrounded a large peristyle courtyard (**Fig. 5**), referred to hereafter as the "atrium unit" and the "peristyle unit" respectively. The northern level, though partially excavated, has not undergone sufficient study to definitively ascertain its characteristics.

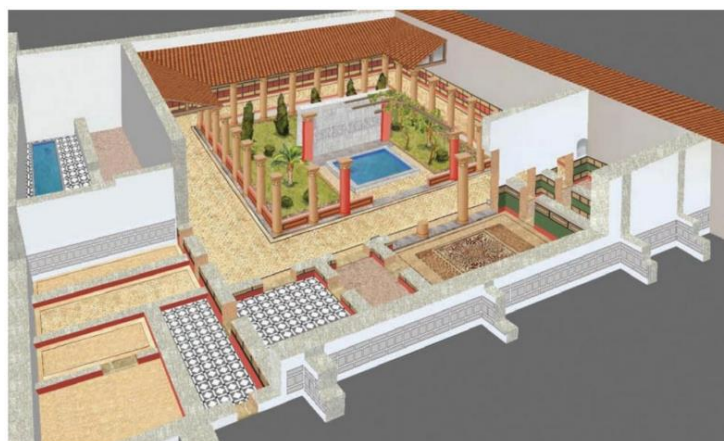


**Figure 5.** The peristyle courtyard.

In the center of the peristyle courtyard unit lies a yard surrounded by stēvi. The southern wing of the rooms faces the courtyard and the pool, including a large portico and four rooms, two on each side of it. The portico mosaic, with its facade facing the pool, was covered in marble slabs which were decorated with figurative reliefs. Soil discovered in the yard contained abundant organic matter, suggesting that this particular area likely served as a garden. During this phase, the planks were adorned with a white mosaic bordered by a black frame, intricately woven with delicate cross-like flower patterns. The walls of the panel exhibited decorative swirls in black, red, and varying shades of yellow towards the lower section, with the colored slabs showing signs of weathering. Additionally, a greenish hue was noted in the partition. Fragments discovered on the floor indicated that the upper wall paintings featured motifs of vegetation and winged figures (**Fig. 6**). The planks were topped with a wooden roof and covered in painted stucco displaying hues of purple and green. On the reverse side of the fragments, two rectangular rugs were observed, flanking a large medallion within a square. This medallion showcased a black and white pattern reminiscent of the mosaic discovered in the living room of the multistory building beneath San Paolo alla Regola in Rome (Portella, 2007). Notably, the Roman mosaic dates back to the Flavian period (69–96 AD), coinciding with the period of the House of the Dioscuri.











**Figure 6.** Fresco fragments from the wall and ceilings.





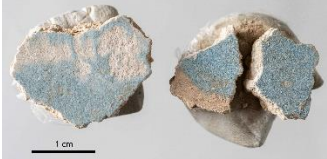


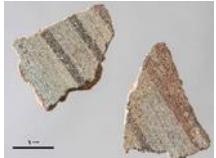
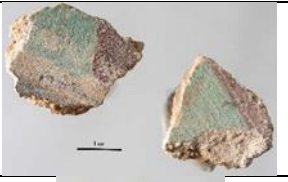

## 5. Materials and methods








### 5.1 Sample description

A total of 21 fragments of wall paintings were collected, 15 originating from Motza (MF1-MF15) and 6 from Caesarea (CF1-CF6). After macroscopic observation, selected samples were collected from each fragment in order to have a complete representation of all the different pictorial colors and characteristics. The samples were classified based on the color of their pictorial layers into five distinct groups: yellow, green, blue, red, and black. For samples displaying a multicolored paint layer, we opted to categorize them into the group that reflects the most predominant color, however during the analysis phase, each color will be addressed individually. In the table below (**Tab.1**) each group is presented, along with photos and notes for each sample.

**Table 1.** Sample groups, photos and notes.

Predominant color-Group	Sample	Photo	Note
Yellow-1	MF1		dark yellow/mustard surface, with a horizontal purple stripe
	MF2		nude surface with a red horizontal overpainting on the upper section and a yellow one closer to the middle
	MF6		nude surface with brown and yellow overpaintings
	MF11		darker to lighter yellow and red shaded stripes
	CF6		weathered yellow
Green-2	MF7		turquoise
	MF8		red with a small green overpainting
	MF9		green and grey

	MF10		green, red and black (left), green and red (right)
	MF13		dark green
	MF14		light/dark green and dark red
	CF5		green and grey
Blue-3	MF4		light blue
	MF5		blue, dark/light green stripes (left), dark/light green and red
Red-4	MF2		-
	MF5		-
	MF10		-
	MF11		-

	MF12		light red/pinkish shade
	MF15		dark red with grey spots
	CF1		light red/pinkish shade
	CF2		light red/pinkish shade
	CF3		red/pinkish shade, slightly darker
	CF4		orange
Black-5	MF3		-

### 5.2 Sample preparation

The samples were prepared in cross sections and all subsequent analyses were carried out using those cross sections, excluding XRD/XRPD. For XRD/XRPD analyses, a distinct preparation method was employed, which will be described further below.

The cross sections were prepared in the facilities of the Department of Geosciences at the University of Padova. The process began by positioning the fragments with a vertical orientation of the pictorial layer into rectangular molds (**Fig.7**), followed by the meticulous preparation and pouring of Araldite 2020 resin and hardener mixture into the containers. Subsequently, the filled containers were carefully transferred into a vacuum chamber to eliminate any trapped air within the samples, ensuring optimal resin

penetration. After the vacuum process, the samples underwent curing in an oven until fully dry. Upon completion, the cured embedded samples were meticulously prepared by gritting them with abrasive papers until the painting layer was fully visible and horizontal, followed by a thorough polishing phase.



**Figure 7.** Samples of fragments placed in molds, before the pouring of resin, Department of Geosciences, Padova, Italy.

Following this preparation procedure, 22 cross section samples were prepared for the site of Motza, labeled with MF1-MF15 and 8 for Caesarea, labeled as CF1-6. Those with the appendixes i/ii, refer to samples taken from the same fragments but regions of them that display different colors or shades.

The complete list of the samples and the analytical procedures they underwent is summarized in the following table. The notes are intended to depict special color characteristics of the samples with appendixes.

**Table 2.** Complete list of cross section samples.

Sample name	Group	Notes	PLM	micro-Raman	SEM-EDS	XRD-XRPD
MF1i	1	mustard part	x	x		
MF1ii	4	purple stripe	x	x	x	x
MF2i	4	upper red part	x	x		
MF2ii	1	middle yellow part	x	x	x	
MF3	5	-	x	x	x	x
MF4	3	-	x	x		x
MF5i	3	dark/light green and blue	x	x	x	x
MF5ii	3	green/blue and red	x	x		
MF6	1	-	x	x		

MF7i	2	dark turquoise	x	x		
MF7ii	2	light turquoise	x	x	x	
MF8	2	-	x	x	x	x
MF9i	2	green and grey	x	x	x	x
MF9ii	2	green	x	x		
MF10i	4	black, non-colored and red	x	x	x	x
MF10ii	4	green and red	x	x		
MF11	4	-	x	x		
MF12	3	-	x	x		
MF13	2	-	x	x		
MF14i	2	dark green and red	x	x		
MF14ii	2	light/dark green	x	x	x	
MF15	4	-	x	x	x	x
CF1	4	-	x	x	x	
CF2	4	-	x	x		
CF3	4	-	x	x		
CF4	4	-	x	x		
CF5i	2	grey	x	x	x	
CF5ii	2	green	x	x		
CF6	6	-	x	x	x	x

### 5.3 Optical microscopy (PML)

Optical microscopy is a technique commonly used in a complementary manner in most cases along with SEM-EDS for micro-stratigraphic analysis of painted surfaces (Cornale *et al.*, 2005; Regazzoni *et al.*, 2018). Microscopic examination of the interface between the preparation and the paint layer serves as the primary criterion for differentiating between fresco and secco painting techniques. A seamless transition between these layers indicates the application of the fresco technique, whereas a distinct separation between the ground and the initial paint layer suggests the use of the secco technique (see **Chapter 2**). Furthermore, optical microscopy observations help to analyze the paint layer's properties, including the identification of any lumps, the sample's stratigraphy, and assess the plaster characteristics.

Polarized Light Microscopy (PLM) in transmitted light (TL) under a Leica DM750 P operating with an integrated digital camera FLEXACAM C1 (Leica Microsystems, Heerbrugg, Switzerland) was used.

### 5.4 Micro-Raman spectroscopy

Raman spectroscopy is a non-invasive technique that has proven valuable in analyzing the molecular composition of materials found in archaeological artifacts and artworks. It stands out as a fitting tool for this task, offering crucial insights at the microscopic scale, while aiding in conservation efforts, restoration projects, and dating endeavors related to wall paintings and other forms of art (Baraldi *et al.*, 2001; Hernanz *et al.*, 2008; Perez-Rodriguez *et al.*, 2014).



**Figure 8.** Micro-Raman spectrometer,  
Department of Chemistry, Padova

Raman spectra were collected using on the cross sections a Thermo Scientific DXR Micro-Raman spectrometer (Thermo Fisher Scientific, Waltham, MA, USA) equipped with 10x and 50x-LWD objectives (**Fig.8**). We used the laser working at 532 nm and power of 6-9 mW. The spectra were obtained by averaging 64 scans recorded from 105 to 3500  $\text{cm}^{-1}$  with 2.7–4.2  $\text{cm}^{-1}$  spectral resolution and 1 s of recording time. Different points of the sections were analyzed in order to identify the chemical composition of the pictorial layer and the mortar. Spectra were collected and treated with OMNIC for Dispersive Raman software (Thermo Fisher Scientific, Waltham, MA, USA). The analysis procedure was conducted in the laboratories of the Chemistry Department of the University of Padova.

#### *5.5 Scanning Electron Microscopy – Energy Dispersive Spectroscopy (SEM-EDS)*

Scanning electron microscopy is used as a powerful tool to investigate the stratigraphy of paintings and the elemental composition of artifacts (Vančo *et al.*, 2013; Pronti *et al.*, 2020).

13 selected samples of the cross sections were selected to be further analyzed under scanning electron microscopy (see **Tab.2**). The selection process was based on the results obtained by previous analyses, specifically choosing samples whose composition was not clearly defined, such as the green and blue samples that mostly presented a weak or insufficiently defined Raman signal. Additionally, certain samples were chosen to validate micro-Raman results. The preparation process for SEM-EDS analysis involved coating the cross sections with a fine layer of gold using the Quorum Q150R rotary pumped coater via a sputtering procedure (**Fig. 9**).





**Figure 9.** Quorum Q150R, Chemistry Department, Padova.

This coating step was essential to enhance the spatial resolution of the acquired images, leveraging the conductive properties of gold. The prepared samples were analyzed using the COXEM EM 30AX plus located in the CEASC laboratory of the University of Padova, equipped with a tungsten cathode and a four-quadrant solid state BSE for imaging. The analysis was carried out in BSE (Backscattering Electrons), an acceleration voltage of 20 kV; filament current 1.80 A; emission current 20  $\mu$ A; aperture current 300 nA and working distance 11-13 mm. The chemical composition of the samples was obtained using the energy dispersive X-ray detector (EDX) EDAX Element-C2B, while qualitative interpretation of the spectra and semi-quantitative chemical analysis were performed through the TEAM<sup>TM</sup> EDS Analysis System. The analytic procedure took place in the Department of Chemistry laboratories of the University of Padova.

#### 5.6 X-ray diffraction (XRD) – X-ray powder diffraction (XRPD)

X-ray diffraction (XRD) is an analytical technique commonly applied for archaeometric studies, providing mineralogical composition of the analyzed sample (Artioli, 2010; Uvarov, Popov and Rozenberg, 2015; Secco *et al.*, 2020).

This technique was used both in a non-destructive and destructive way. For the former, fractions of the fresco fragments were directly analyzed on the surface in order to investigate the pictorial layer. Those samples consisted of 2 blue ones (MF4, and MF5), 1 yellow (MF1), 2 green (MF9 and MF10), 2 red (MF15 and CF1) and 1 black (MF3). For the analysis of the mortars, 2 samples from Motza (MF8 and MF15) and 1 from Caesarea (CF6), were chosen and analyzed by XRPD (X-ray Powder Diffraction). Portion of the selected samples were subjected for the initial grinding using a pestle and mortar to achieve a fine powder consistency (**Fig.10,a**). Subsequently, the powder was thoroughly mixed with 20 wt% of a standard, zinc oxide (ZnO). This standard serves as an internal reference to detect instrumental errors such as sample displacement and

to quantify the amount of amorphous phase by adjusting the quantity of crystalline components (internal standard method).



**Figure 10.** a) Powder of 0.8g of sample, grinded using pestle and mortar, b) Sample fragments placed on metal disc, ready to be set in the diffractometer. Department of Geosciences, Padova.

The XRD analysis took place in the department of Geosciences at the University of Padova, using a Malvern PANalytical X'Pert Pro diffractometer in Bragg-Brentano geometry. Data acquisition was carried out under Co Ka radiation by the use of a continuous scan in the range  $3-85^{\circ} 2\theta$ , a virtual step size of  $0.017^{\circ}$  and 100 s counts per step for the samples that needed no preparation. For the samples in powdered form MF4 and CF6, the conditions were slightly different, with a range of  $3-90^{\circ} 2\theta$ , step size  $0.03^{\circ}$  and 300 s per step. For the interpretation of the data and the identification of the mineral phases the X'Pert HighScore Plus was utilized along with international databases, such as the ICDD (International Centre for Diffraction Data) which provides standard diffractograms for the comparison of known mineralogical phases.

## 6. Results and discussion

### 6.1 Optical microscopy (PLM)

Following the comprehensive description of the samples in **Chapters 5.1** and **5.2**, this chapter will focus on investigating their micro stratigraphy and utilized painting techniques. In the following table there is a summary of all the samples and the number of layers for each one of them along with the painting technique employed.

**Table 3.** Samples, number of layers and painting techniques of all the analyzed samples.

Sample name	Group	Number of layers	Notes/Colors	Painting technique
MF1i	1	1 or 2	1. Yellow 2. Light brown (in some areas)	fresco
MF1ii	4	2	1. Yellow 2. Thin dark red to black	fresco and secco
MF2i	4	1	Red	secco
MF2ii	1	3	1. Whiteish 2. Yellow 3. Light brown (in some areas)	secco
MF3	5	1	Black	secco
MF4	3	1	Light blue	secco
MF5i	3	1 or 2	1. Pale blue / yellow 2. Very light almost transparent blue-green / thin dark	secco
MF5ii	3	1, 2 or 3	1. Very light blue / yellow 2. red/light blue-green 3. Brownish (some areas)	secco
MF6	1	1	Yellow-orange	secco with yellow lumps in plaster
MF7i	2	1	Dark green almost black	secco
MF7ii	2	1 or 2	1. Light green 2. Whiteish (some areas)	secco

MF8	2	1 or 2	1. Red 2. Dark blue-green	fresco and secco
MF9i	2	2	1. Red 2. Green-grey	fresco and secco
MF9ii	2	2	1. Very light green 2. Thin black	secco
MF10i	2	2 or 3	1. Black/red/green 2. Whiteish/red 3. Yellow in the plaster in some areas	secco
MF10ii	2	1, 2 or 3	1. Red/orange 2. Light green 3. Red/orange	fresco and secco
MF11	4	1 or 2	1. Yellow 2. Red	secco
MF12	4	1 or 2	1. Red 2. Light brown	fresco and secco
MF13	5	1	Black	secco
MF14i	2	1 to 3	1. Dark green/red 2. Red 3. Light green-whiteish	fresco and secco
MF14ii	2	2 or 3	1. Dark green 2. Light green 3. Brownish (in some areas)	fresco and secco
MF15	4	2	1. Very thin red and black 2. Whiteish	secco
CF1	4	3	1. Lighter plaster 2. Orange-red 3. Dark brownish	secco
CF2	4	2	1. Light red-orange 2. Brownish (in some areas)	secco
CF3	4	3	1. Lighter plaster 2. Orange-red 3. Dark brownish	secco
CF4	4	3	1. Lighter plaster 2. Orange-red 3. Dark brownish	secco
CF5i	2	1 to 5	1. Lighter plaster 2. Greyish 3. Green	secco

			4. Whiteish 5. Grey	
CF5ii	2	2	1. Greyish 2. Green	secco
CF6	1	1	Greyish with yellow tones	secco

In general, the way of layering in the pictorial layers is discernible and, in most samples, the secco technique has been employed. However, the fresco technique has been used for some samples, mostly for underpaintings. It's interesting to focus on the samples that display multiple or complex layering. Starting with MF1ii, its way of layering reveals the presence of a yellow layer in fresco and an overpainting of dark red and black elements in secco that appears as the purple stripe in the fragment (**Fig.11**). Lumps of yellow pigment in multiple sizes can also be distinguished.

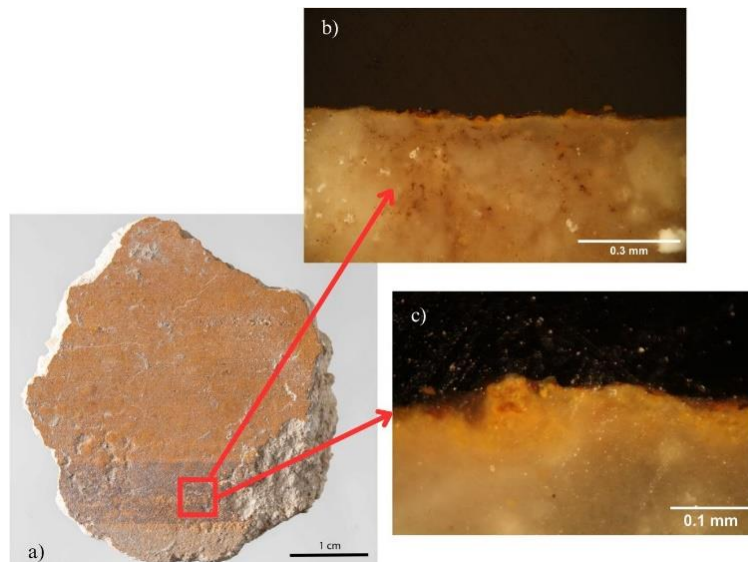


**Figure 11.** Sampled area of MF1ii cross section from MF1 fragment (a), microscope photos of the sample's stratigraphy (b,c).

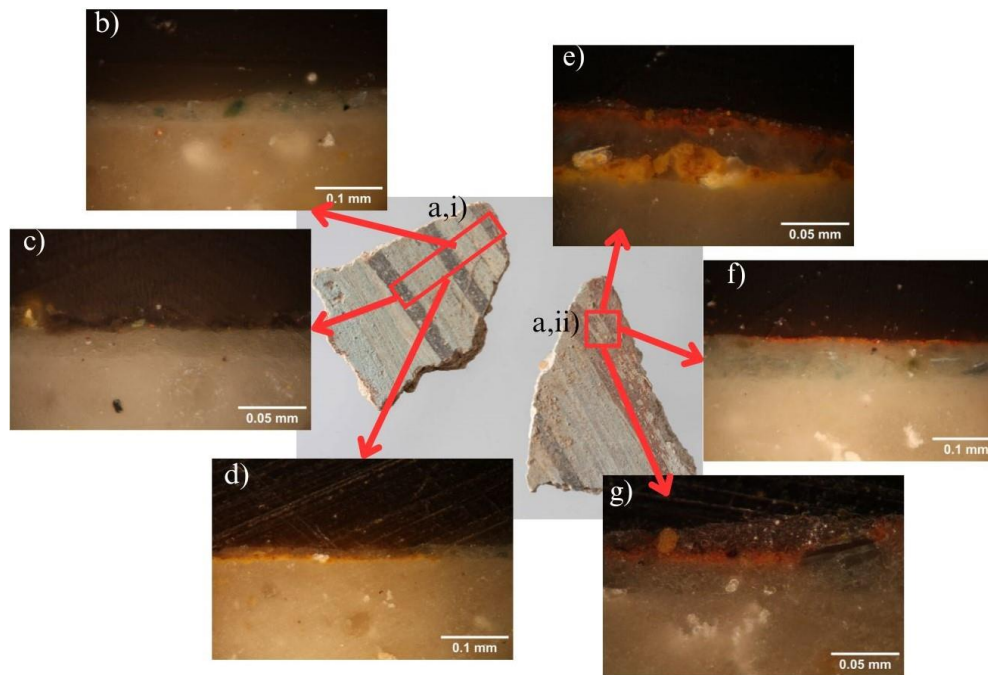


**Figure 12.** Sampled areas of MF5i (a(i),b,c,d) and MF5ii (a(ii),e,f,g), with microscope photos indicating each sample's stratigraphy.

The samples MF5i and MF5ii (described in **Fig.12**) show a single layer of very light blue with green and blue lumps of pigments that is applied in secco (**Fig.12,b**). Furthermore, there is a very light blue layer but with the addition of a dark green to black overpainting, both applied in secco (**Fig.12,c**). This dark layer is probably referring to the dark green stripe of the fragment. Lastly, a yellow underpainting in a part of the green area between the stripes, also in secco, can be discerned (**Fig.12,d**). This finding is interesting because it is not visible with the naked eye, and that yellow layer was used as a preparatory layer. The same preparatory layer is found in MF5ii (**Fig.12,e**). In the next photo (**Fig.12,f**), the same pale blue layer can be observed, accompanied by a delicate red layer applied in secco, matching the red areas of MF5ii. Additionally, in the last picture (**Fig.12,g**), aside from these layers, there is another nearly brown one with a yellowish lump, likely due to dirt buildup.

An intriguing case study emerges with the sample MF9 (**Fig.13**). Specifically, the grey area of the sample that is represented by MF9i (**Fig.13,c,d**), although not visible macroscopically except in a small area at the right corner of the grey part of the fragment, is characterized by the presence of a red underpainting applied in fresco. This layer is absent in MF9ii (**Fig.13,b**), where only the green portion of the fragment is depicted. Instead, in this instance, a sole light green layer is discernible, occasionally accompanied by a faint black layer in select areas. Following this, a red preparation layer was applied in fresco specifically for the grey area of the sample, over which a very light green to grey painting layer was applied in secco. This strategic layering suggests an intentional choice by the artist, as contrasting colors often serve as underpaintings to enrich the final hues or add depth to the composition. In addition, concerning the green portion of the fragment, apart from the single light green layer applied in secco, some areas exhibit a thin black layer that is likely attributed to either accumulated dirt or visible surface irregularities present on the MF9 fragment.

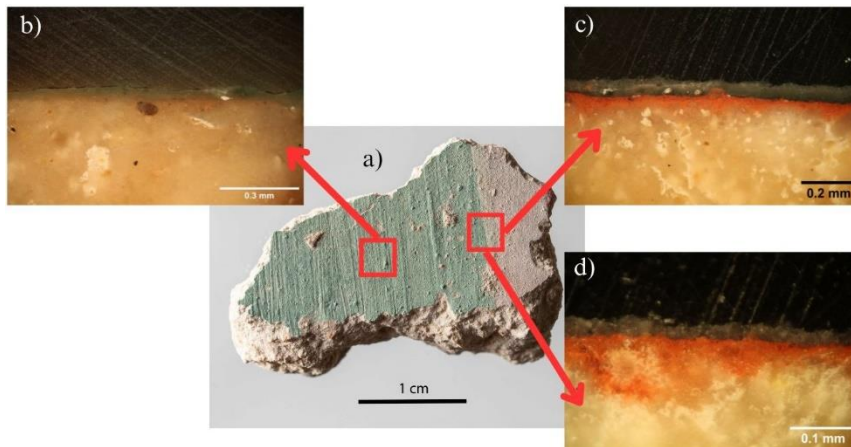


**Figure 13.** Sampled areas of MF9, with microscope photos indicating the sample's stratigraphy.

Noteworthy is the stratigraphy presented in sample MF10 (**Fig.14**). Starting with MF10i (**Fig.14,a(i)**), this is characterized by the presence of 2 or 3 layers. The first one corresponds to the black weathered area of the first fragment, a fact that can be observed by the black layer that is visible in some areas and not in others, especially when the white layer of plaster is on top (**Fig.14,b**). Interestingly, the plaster underneath this black layer has a yellow tone with some small yellow particles. In the red part of the fragment a single red layer along with a thin brownish one related to dirt are observed (**Fig.14,c**), while in the same area there is a red overpainting above the green layer, uncovered in other areas of the sample. In the former areas, a yellow layer inside the plaster, close to the pictorial layer is observed (**Fig.14,d**).

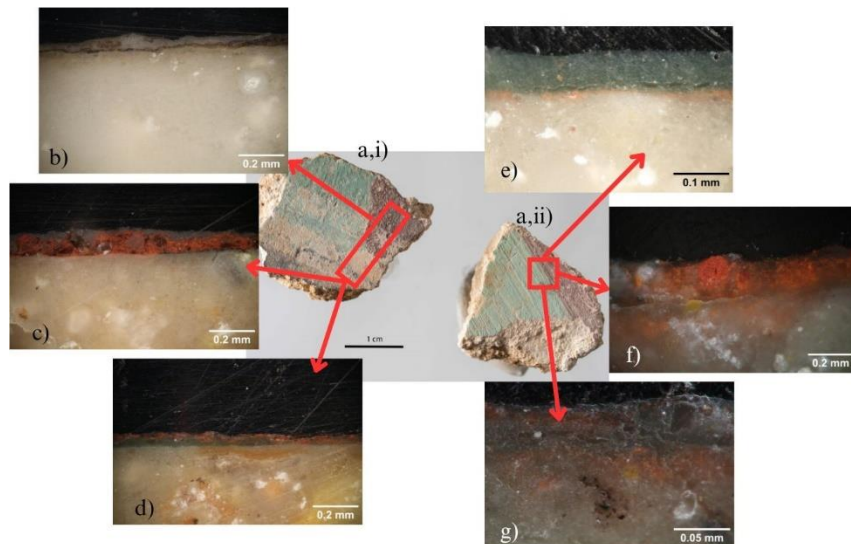


**Figure 14.** Sampled areas of MF10i (a(i),b,c,d) and MF10ii (a(ii)e,f,g), with microscope photos of each sample.

Accordingly, in MF10ii, a layer of light green can be observed (**Fig.14,e**), with a very thin layer of red underpainting. The green is applied in secco, however the red in some areas may have been applied in fresco, as the pigment has the appearance of seeping into the mortar (**Fig.14,f,g**).

MF14 (**Fig.15**) is a sample that exhibits multiple layers, namely a dark green preparatory one, and a red overpainting for MF14i, only in red colored areas (**Fig.15,b**), while in others only the dark one is present (**Fig.15,c**). Similarly, in the upper area of the fragment (**Fig.15,a(ii)**), the dark green preparatory layer is present, followed by a lighter green one (**Fig.15,d**). Above this layer, a brown one is observed in some parts of the sample that looks like aggregate that has been placed on top of the pictorial layers.

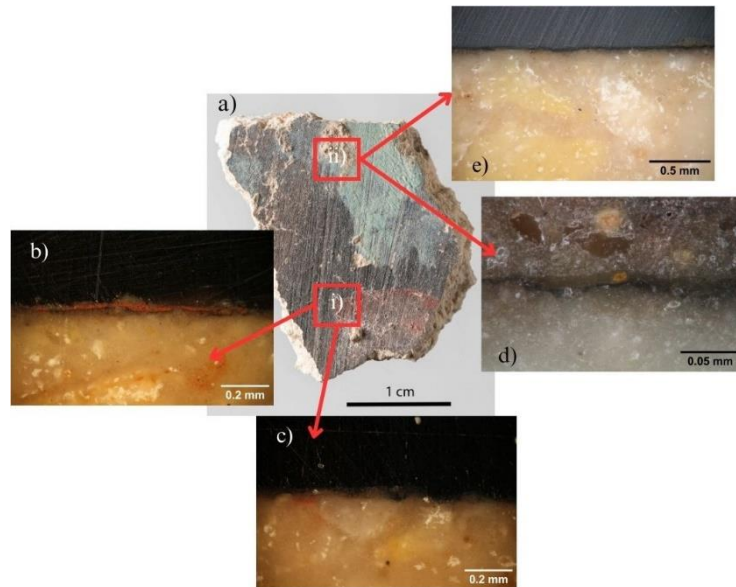


**Figure 15.** Sampled areas of MF14i (a(i)) and MF14ii (a(ii)), with microscope photos of each sample.

For the samples from Caesarea, CF1, CF2, CF3 and CF4, those exhibit almost the same kind of stratigraphy (**Fig.16**). In particular, a preparatory layer of lighter mortar is featured in all the samples from Caesarea. This layer serves the purpose of enhancing the vibrancy of colors and creating a smoother surface conducive to color application.

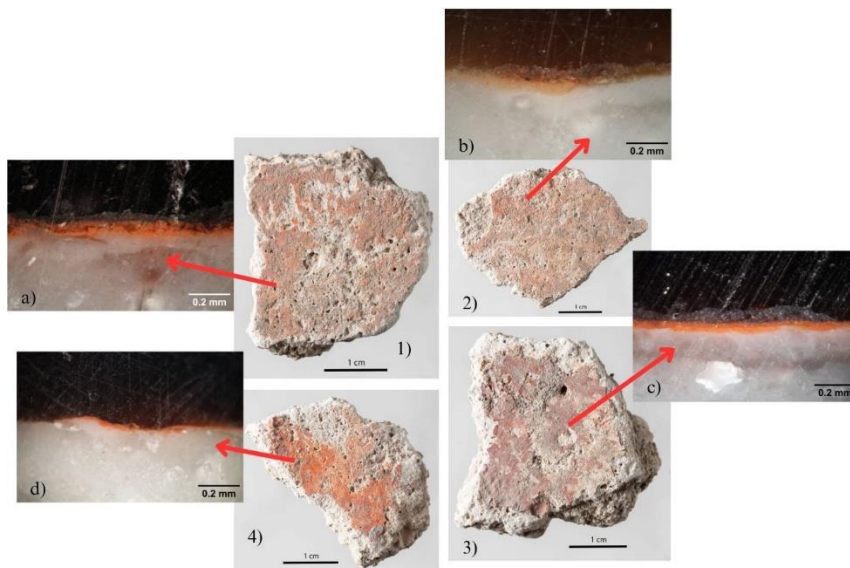


**Figure 16.** Samples CF1(1), CF2(2), CF3(3) and CF4(4), with microscope photos of each sample (a,b,c,d).



Furthermore, the first pictorial layer is a vibrant red one in CF1 and CF3 applied in secco (**Fig.16,a,c**), followed by a brown one related to dirt buildup. For CF2, a yellow weathered sample, a very light orange to yellow layer is evident, with the addition of the brown one (**Fig.16,b**). Lastly, CF4 features a layer of orange consistent with the color of the fragment (**Fig.16,d**). All the layers in those fragments, as described in **Tab.1**, are applied in secco.

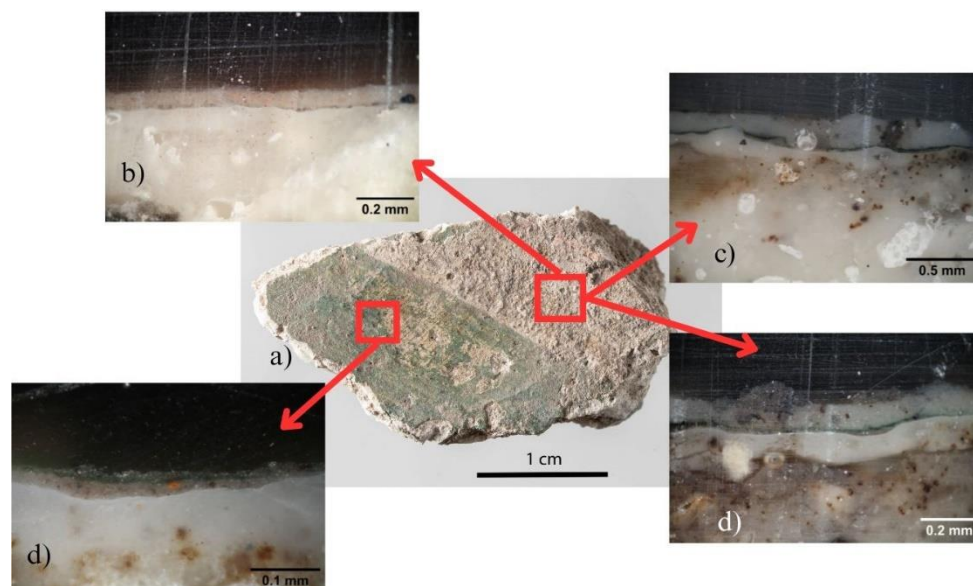


**Figure 17.** Sampled area of CF5i (a), with microscope photos of the sample (b,c,d).

Moreover, a sample with a noteworthy stratigraphy is CF5i, which is derived from the grey area of CF5 (**Fig.17**). This sample in some areas features a single light grey layer (**Fig.17,b**). In others, however, a total of 5 layers are present. First, there is the lighter preparatory plaster layer present in all of Caesarea samples. Then, a very thin grey one is observed, followed by an equally thin green one. Finally, another layer seemingly of the same lighter plaster as the first one is applied, followed by another very thin grey one in some parts of the sample (**Fig.17,c**). All the layers look like they are applied in secco. This type of layering suggests that the light preparatory plaster and thin grey layer of pigment could have been applied to provide a base for the green-colored layer, while the reappearance of plaster followed by a grey layer may indicate repairs or alterations made over time. Also considering the other half of the fragment (**Fig.17,d**), there is a possibility that the whole wall was painted green and then there was the addition of plaster with the grey colored layer on top for this side of the wall to be grey.

In addition, other than the microscope photos, image stitching was used for each one of the samples in order to have a clear picture of the cross sections and observe not only the pictorial layer but also the mortar characteristics. Starting with the Motza samples (**Fig.18**), those appear to have one layer of *intonaco*, the final layer of plaster on top of which the paint is applied, usually the finer particle size plaster used for pigment application. In some samples, like MF6, MF11 and MF13 the *arricio* is also visible, a layer applied on the wall with a rougher texture than *intonaco*, intended as a base for it. In all of Motza samples we can observe a plaster of generally the same grain size of

aggregate, no layering and an overall homogenous appearance, except than MF15 which features a large white aggregate particle.

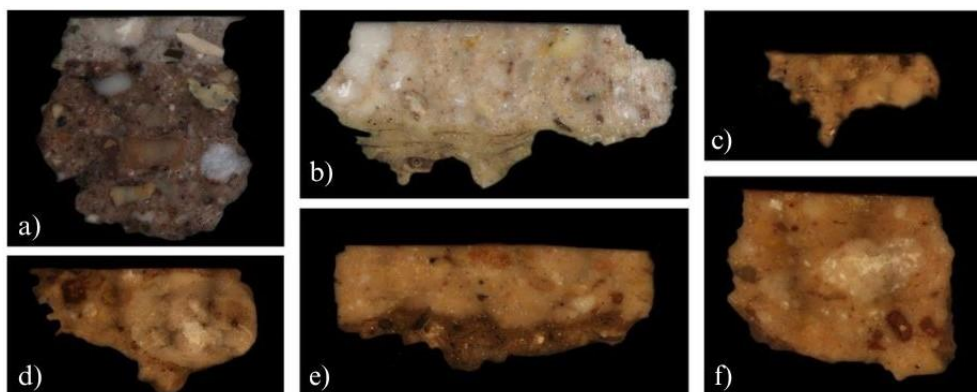


**Figure 18.** Samples from Motza showcasing their mortar's stratigraphy. MF13(a), MF10i(b), MF1ii(c), MF8(d), MF6(e), MF9i(f).

On the other hand, Caesarea samples (**Fig.19**) feature a more complex kind of substrate than the Motza ones (**Fig.19**). Specifically, a layering in the plaster can be observed, at the lower part with a thick layer of mortar consisting of shell and rock fragments, likely identified as the local *kurkar* that was mentioned in earlier chapters, a calcareous sandstone. This layer obviously contains shell fragments. On top of this rough textured kind of *arriccio*, there is a homogenous layer of *intonaco*, much smoother in texture and ideal for the application of the paint layer. In addition, an interesting feature of CF6 is the presence of an almost black rock with a layer of red pigment, that is likely to suggest the reuse of frescoes in plaster production.

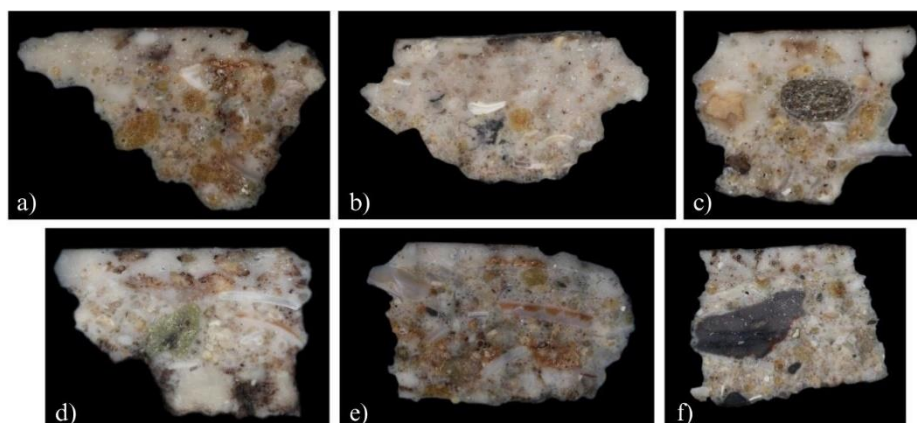


**Figure 19.** Samples from Caesarea showcasing their mortar's stratigraphy. CF1(a), CF5i(b), CF2(c), CF5ii(d), CF4(e), CF6ii(f).

## 6.2 micro-Raman spectroscopy

In this chapter, we will examine the chemical composition of each pictorial layer of the samples, organized by the previously mentioned groups. Using micro-Raman spectroscopy, we obtained crucial results that provided not only detailed chemical profiles of the samples but also valuable insight for planning subsequent analyses.

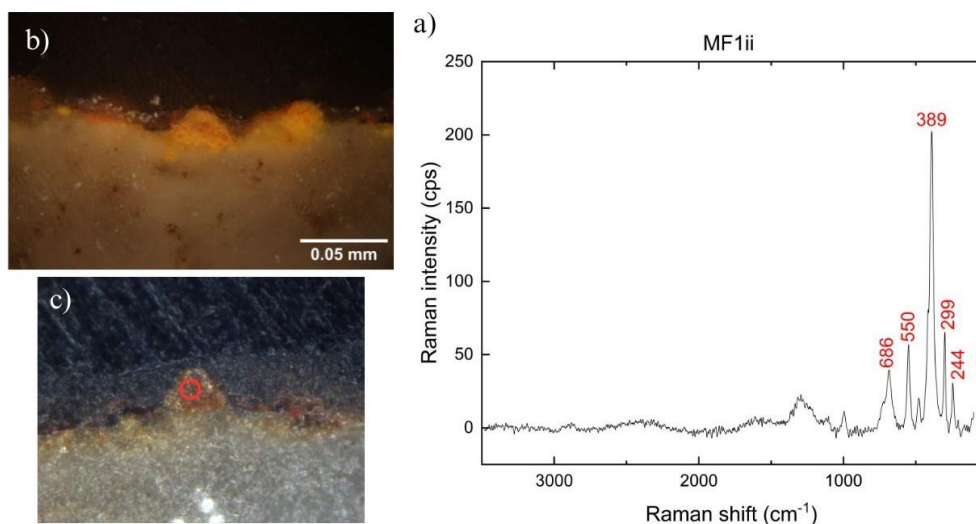


**Figure 20.** Image of the area of MF1ii sample where the beam was directed (red circle in c), from the optical microscope (b) and Raman instrument (c).  $\mu$ -Raman spectrum of the yellow particle (a) showing typical goethite bands.

The first group (yellow samples) shows the presence of goethite ( $\alpha$ -FeOOH, iron oxide hydroxide), which is the chromophore mineral of the yellow ochre. **Fig.20.** shows the Raman spectrum obtained from the yellow lump in the MF1ii sample, highlighting the characteristic bands of goethite. Goethite can be identified by the narrow doublet at  $299\text{-}389\text{ cm}^{-1}$  corresponding to symmetric Fe–OH stretching vibration and peaks at  $244\text{ cm}^{-1}$  (symmetric Fe–O stretching vibrations),  $550\text{ cm}^{-1}$  (antisymmetric stretching vibration of the Fe–OH bonds) and  $686\text{ cm}^{-1}$  (symmetric Fe–O stretching vibrations) (Hanesch, 2009; Marcaida *et al.*, 2019).

In MF2ii, goethite is identified for the yellow layer (**Fig.21,c**). For the upper white layer, quartz ( $\text{SiO}_2$ ) is identified (**Fig.21,b**). Quartz exhibits a characteristic band at  $465\text{ cm}^{-1}$  (symmetric stretching of O of the six-membered  $\text{SiO}_4$  tetrahedra) (Sharma *et al.*, 2006).

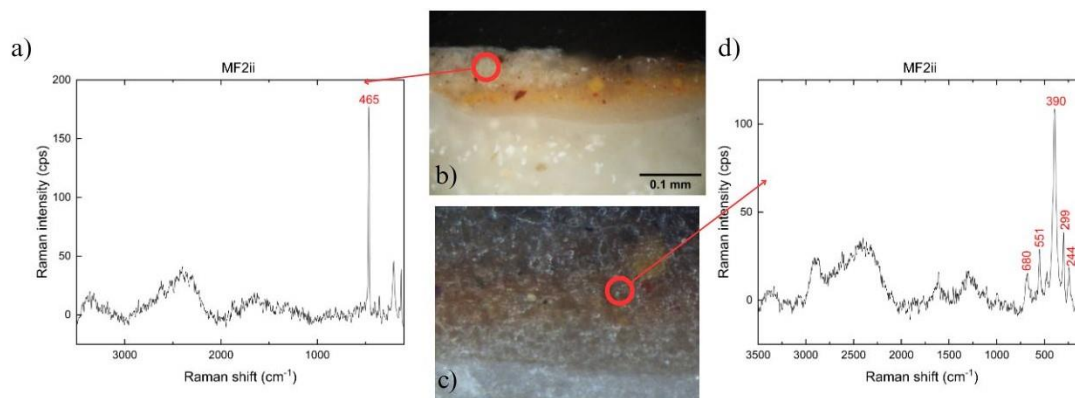


**Figure 21.** a)  $\mu$ -Raman spectrum of the whiteish layer of MF2ii showing the characteristic quartz band, pictured in b) from the optical microscope. d)  $\mu$ -Raman spectrum of the yellow layer showing typical goethite bands, pictured in c) from the  $\mu$ -Raman instrument.

Notably, yellow samples from Motza closely resemble those from Caesarea, showing no significant disparities in their spectra. However, in the weathered yellow sample CF6ii, other than quartz in the orange pigment lump (Fig.22), no other noteworthy findings were observed.

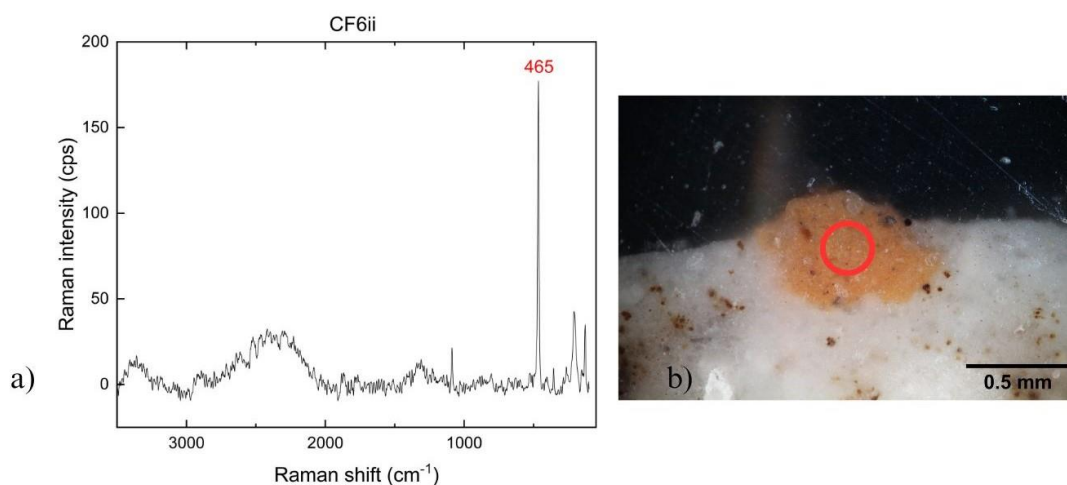


**Figure 22.** a)  $\mu$ -Raman spectrum of the orange pigment lump shown in b) of the sample CF6ii from the optical microscope showing the characteristic band of quartz.

The second group (green samples) exhibited weak Raman signals, consequently providing limited data on their characteristics. Therefore, they were investigated through further analysis, such as SEM-EDS.

Egyptian blue ( $\text{CaCuSi}_4\text{O}_{10}$ ) was identified in the blue lumps of the pigment in the pictorial layer of MF5i sample (third group, blue samples) (Fig.23). Its characteristic bands are present at  $1086\text{ cm}^{-1}$  (symmetric stretching vibration of the Si-O bonds within the tetrahedral silicate ( $\text{SiO}_4$ ) units),  $430\text{ cm}^{-1}$  (vibrational modes involving the bending or stretching of the Cu-O bonds within the copper-oxygen polyhedra) and  $113\text{ cm}^{-1}$  (lattice vibrations within the Ca copper silicate structure) (Baraldi *et al.*, 2001; Jorge-Villar and Edwards, 2021).

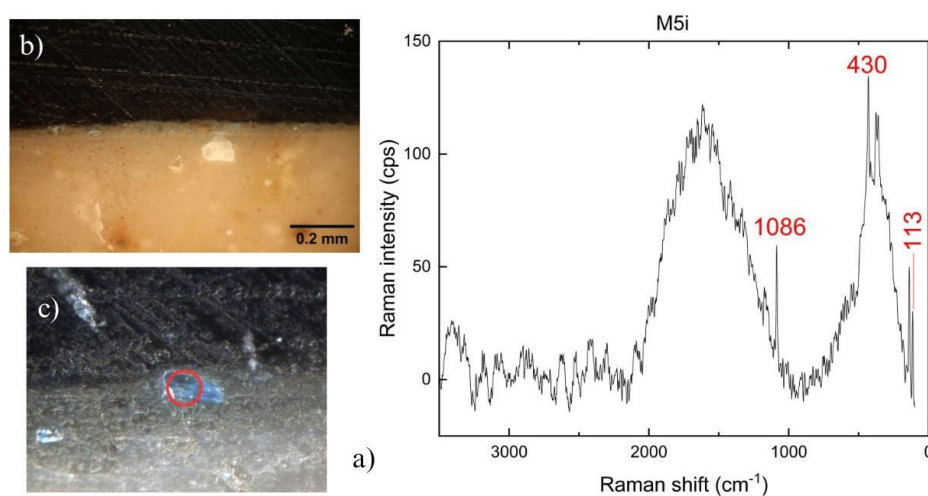


**Figure 23.** a)  $\mu$ -Raman spectra of the blue lump of MF5i indicated in c) from the Raman instrument where the beam was directed. In b) a picture from the optical microscope indicative of the region is shown. The typical bands of Egyptian blue are shown.

Calcite ( $\text{CaCO}_3$ ) might also be present in the blue samples, with its characteristic band at  $1086\text{ cm}^{-1}$  (**Fig.23,a**) overlapping that of the Egyptian blue (Donnelly *et al.*, 2017).

The red samples, belonging to the fourth group, from both Motza and Caesarea, display consistent data with each other. In particular, hematite ( $\text{Fe}_2\text{O}_3$ ), the chromophore mineral of red ochre, was detected in all the red samples, as shown in the red lump of the pigment in MF6 sample reported in **Fig.24**. Hematite is distinguished by its two  $a_{1g}$  symmetric vibrational modes at  $226\text{ cm}^{-1}$  (symmetric Fe-O stretching), and  $496\text{ cm}^{-1}$  (antisymmetric stretching vibration of Fe-O bonds). Additionally, it exhibits five  $e_g$  modes at  $245\text{ cm}^{-1}$ ,  $293\text{ cm}^{-1}$ ,  $299\text{ cm}^{-1}$  (appears as shoulder of the  $293\text{ cm}^{-1}$  band, at room temperature, symmetric bending mode of Fe-O bonds),  $412\text{ cm}^{-1}$  (combination of bending and stretching modes involving both Fe-O and O-Fe-O linkages), and  $613\text{ cm}^{-1}$  (symmetric bending mode of Fe-O). The band at  $1314\text{ cm}^{-1}$  is associated with two-magnon scattering reported in hematite around  $1320\text{ cm}^{-1}$  (Needham *et al.*, 2018; Cosano *et al.*, 2019). The band at  $1085\text{ cm}^{-1}$  can be attributed to calcite, either as part of the ochre or as addition of white pigment.

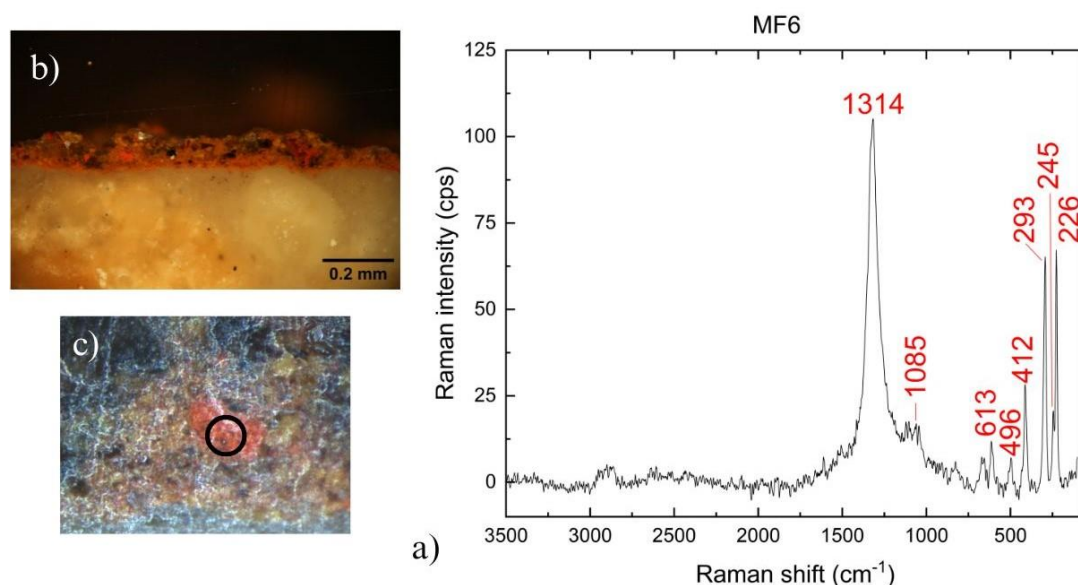


**Figure 24.** a)  $\mu$ -Raman spectra of the red lump of MF6 indicated in c) from the Raman instrument where the beam was directed. In b) a picture from the optical microscope indicative of the region is shown. The typical bands of hematite are shown.

Hematite was identified also with the addition of carbon black in some samples, such as MF10i (**Fig.25**), distinguished by its typical strong bands at  $1599\text{ cm}^{-1}$  (G band or graphite band) and  $1303\text{ cm}^{-1}$  (D band or disorder band) (Secco *et al.*, 2021). Thus, a mixture of red ochre and carbon black have been used to produce this color.

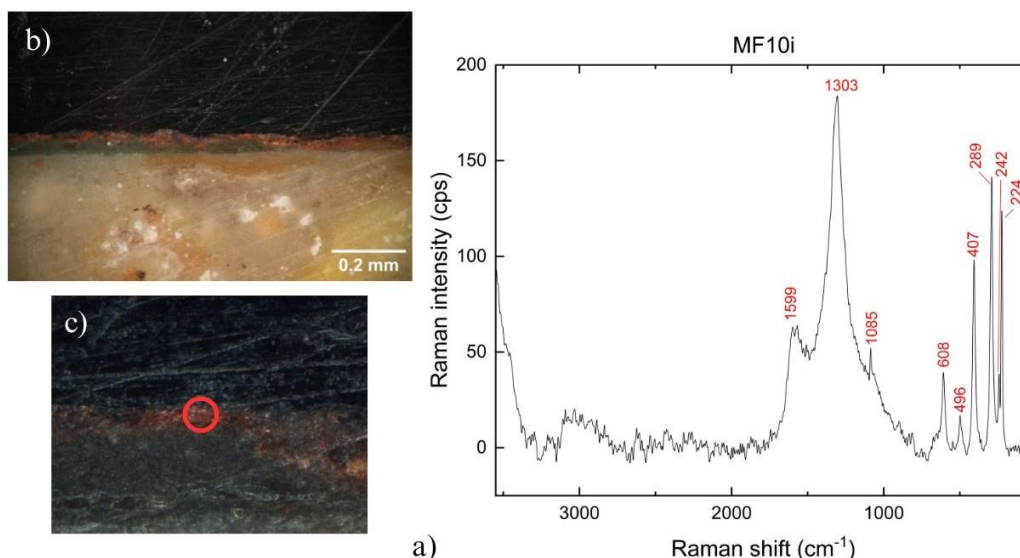


**Figure 25.** a)  $\mu$ -Raman spectra of the red layer of MF10i indicated in c) from the Raman instrument where the beam was directed. In b) a picture from the optical microscope indicative of the region is shown. The typical bands of hematite and carbon black are shown.

In the red sample MF8 (**Fig.26**), litharge was detected. Litharge, a form of lead oxide ( $\text{PbO}$ ), exhibits a characteristic very strong Raman band at  $144 \text{ cm}^{-1}$  (Edwards *et al.*, 2001). Since this was the only sample featuring this characteristic, it has been further analyzed by SEM-EDS to verify the presence of lead. The bands at  $1088 \text{ cm}^{-1}$ ,  $1302 \text{ cm}^{-1}$  and  $1608 \text{ cm}^{-1}$  correspond to calcite and carbon black respectively.

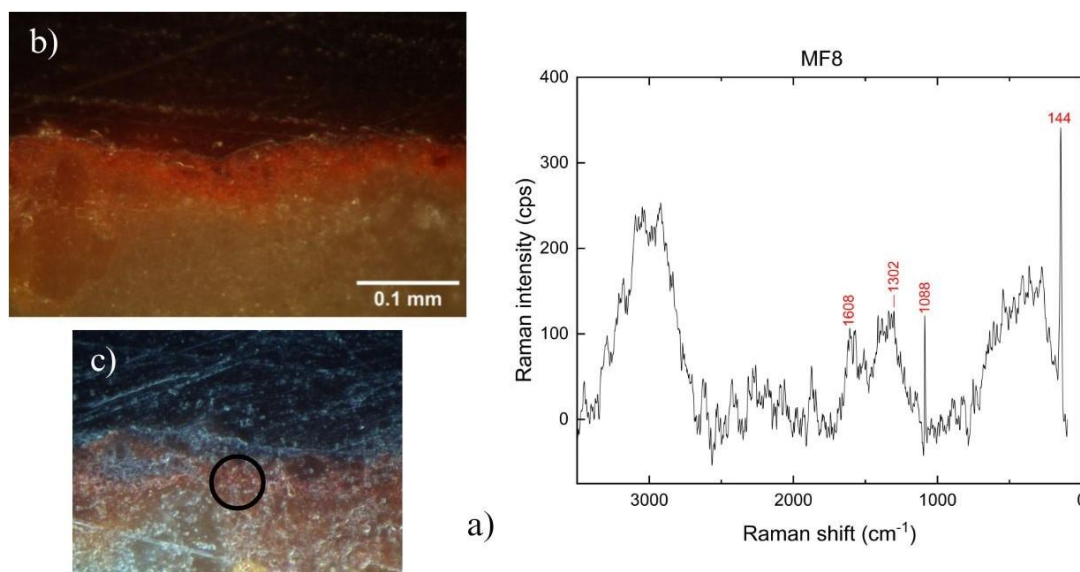


**Figure 26.** a)  $\mu$ -Raman spectra of the red layer of MF8 indicated in c) from the Raman instrument where the beam was directed. In b) a picture from the optical microscope indicative of the region is shown. The typical bands of litharge and carbon black are shown.

Finally, carbon black and calcite were detected in the black sample MF3 (**Fig.27**). The characteristic bands of carbon black at  $1351 \text{ cm}^{-1}$  and  $1604 \text{ cm}^{-1}$  calcite at  $1085 \text{ cm}^{-1}$  shown in **Fig.27,a** suggest a mixture of carbon black and Ca carbonate to obtain the black color. Further investigation by SEM-EDS and XRD were carried out in order to possibly determine the type of carbon black used, such as bone black or ash black.

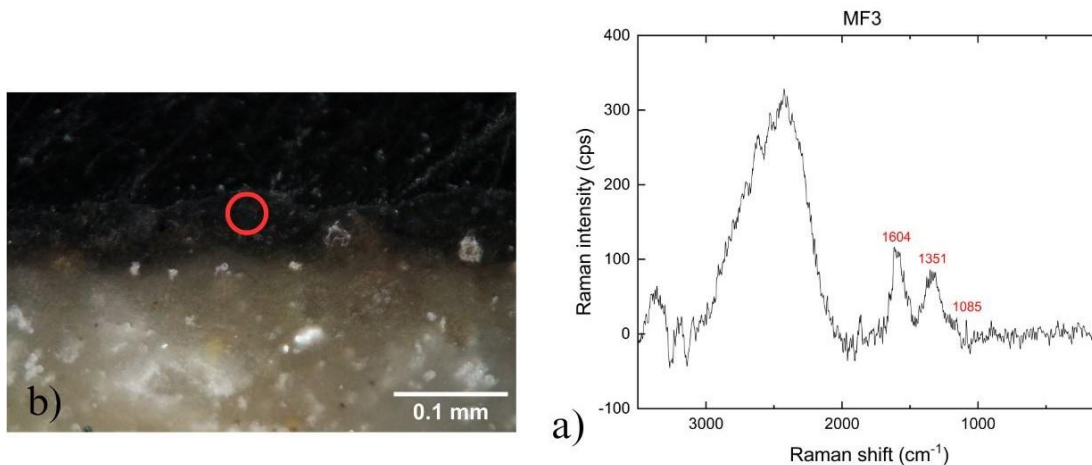


**Figure 27.** a)  $\mu$ -Raman spectra of the black layer of MF3 with a microscope image of the sample MF3 indicating where the beam was directed (b). Characteristic bands of carbon black and calcite are shown.

For reference, the measured Raman bands for the epoxy resin in which the wall fragments were embedded are present at  $3068\text{ cm}^{-1}$ ,  $2918\text{ cm}^{-1}$ ,  $2868\text{ cm}^{-1}$ ,  $1609\text{ cm}^{-1}$ ,  $1458\text{ cm}^{-1}$ ,  $1295\text{ cm}^{-1}$ ,  $1229\text{ cm}^{-1}$ ,  $1185\text{ cm}^{-1}$ ,  $1112\text{ cm}^{-1}$ ,  $949\text{ cm}^{-1}$ ,  $915\text{ cm}^{-1}$ ,  $823\text{ cm}^{-1}$ ,  $772\text{ cm}^{-1}$ ,  $670\text{ cm}^{-1}$ ,  $693\text{ cm}^{-1}$  and  $391\text{ cm}^{-1}$ .

### 6.3 Scanning Electron Microscopy – Energy-dispersive X-ray Spectroscopy (SEM-EDS)

Scanning electron microscopy with energy-dispersive X-ray spectroscopy (SEM-EDS) was applied on a selected group of samples, depending on the results obtained with micro-Raman, as reported in **Tab.2** in **Chapter 5.2**.

The yellow samples (first group) MF1ii and CF6ii were specifically selected to validate the data obtained through micro-Raman analysis and to procure additional insights, respectively. The SEM-EDS results obtained for MF1ii sample, (**Fig.28**) are consistent with those obtained by micro-Raman spectroscopy.

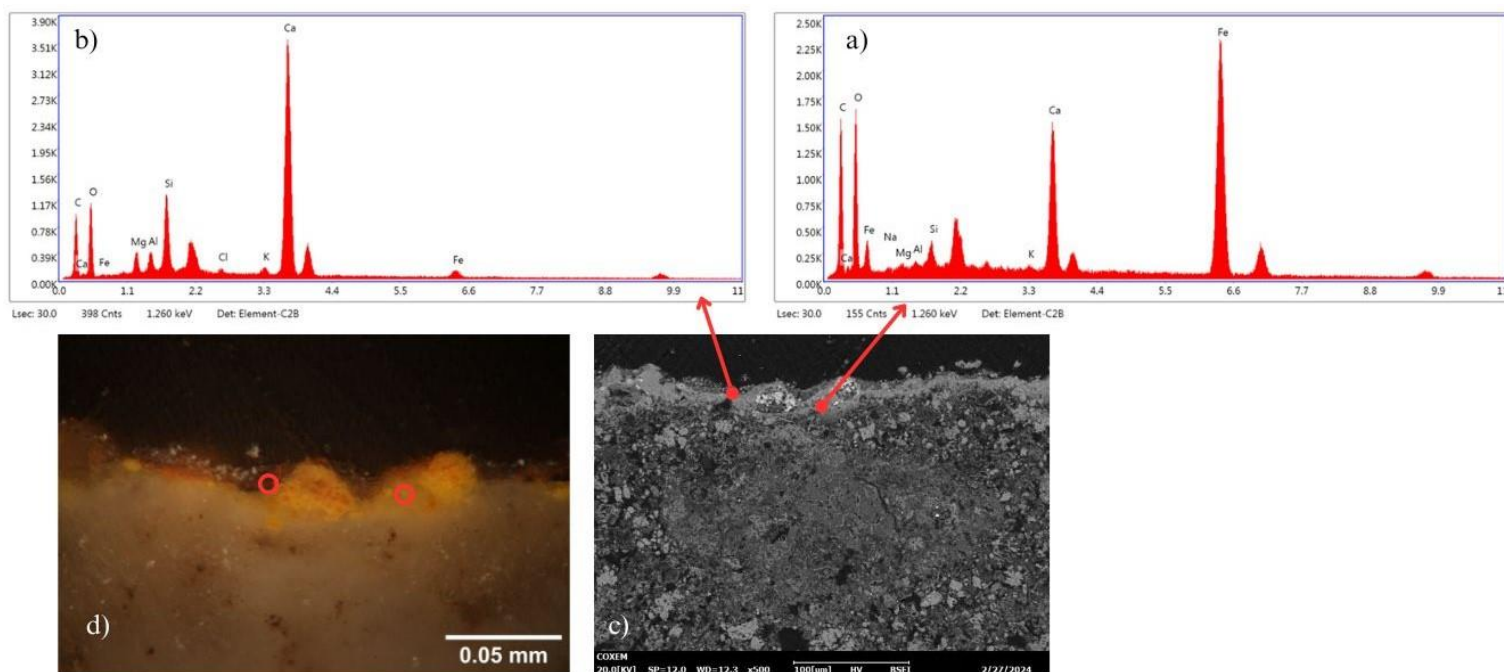


**Figure 28.** a)-b) EDS spectra of the first yellow and second red to black layer of the sample MF1ii. The spectra were obtained from the areas indicated in the SEM (in BSE) (c) and PLM (d) photos.

Through the SEM, the layering that was described in **Chapter 6.1** is clear. The first yellow preparatory layer is relatively thin, applied in fresco and contains coarse-grained particles of the yellow ochre pigment. The fresco application is suggested by the absence of microstructural discontinuities between the plaster and the paint layer (Germinario *et al.*, 2023). In the BSE image (**Fig.28,c**) the pigment grains appear to be coated with a thick film of binder, as their areas look darker and diffused. The second layer of red overpainting is thinner than the yellow, homogenous and applied in secco (Piovesan *et al.*, 2012). EDS revealed a significant proportion of Fe for the yellow layer (**Fig.28,a**), aligning with the characteristic Fe oxide minerals found in yellow ochre pigments, as goethite, which are renowned for their vibrant yellow hues. The elemental composition includes substantial amounts of O, essential for the formation of various minerals and organic compounds within the layer, and Ca, likely derived from Ca carbonate ( $\text{CaCO}_3$ ), related either to the binder or a white pigment mixed in the yellow ochre. The presence of C is additionally related to calcite in this layer. Si can be ascribed to silicate minerals or impurities within the sample substrate. Elements in minor concentrations, like Na, Mg, Al and K could be related to the chemical composition of the mortars or binders, as analyzed and described at the end of this chapter. Cl is likely related to the chemical composition of the epoxy resin, however, it has been found in ochre pigments in relation to a local occurrence of chlorinated salts (Ashkenazi *et al.*, 2021). The second layer, expectedly, has a lower content of Fe and an elevated content of Ca, and can still be associated with red ochre.

Green samples (second group) were analyzed in the SEM-DES, after the inability of the micro-Raman to characterize the type of pigment employed.



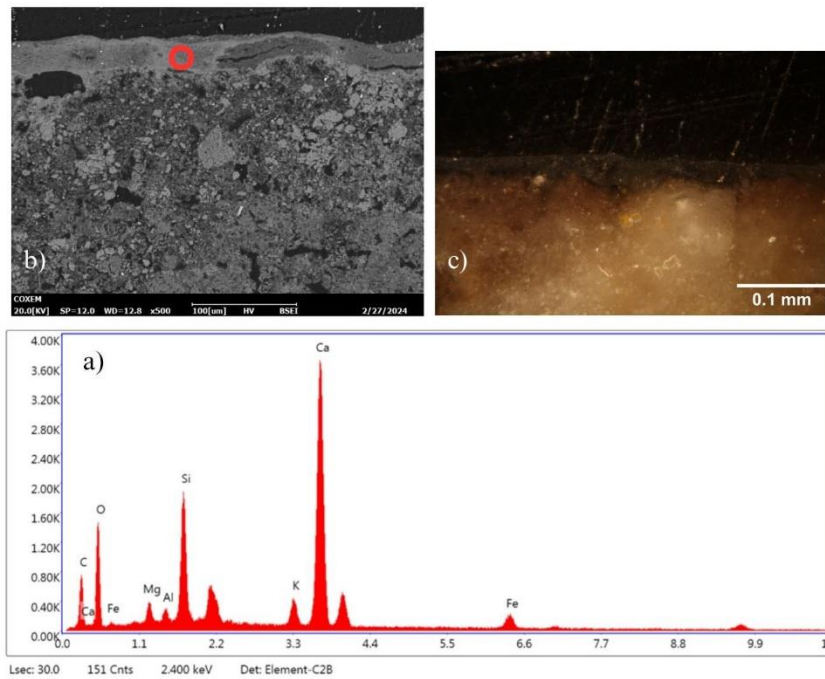


**Figure 29.** a)EDS spectra of the green pictorial layer of sample MF7ii. b) SEM image in BSE of the analyzed area and an optical microscope image of the same area.

Sample MF7ii exhibits a thick homogenous paint layer (**Fig.29,b**). Grains are regularly distributed, while a thin carbonation layer between the plaster and the paint layer can be observed. This indicates that the secco technique was adopted, therefore the pigment was spread on a dry or partially dry substrate. The high concentration of Ca detected by the EDS analysis may also indicate the employment of the *mezzofresco* technique, in which pigments are mixed with limewash (Piovesan *et al.*, 2011). These observations apply in all the green samples, like MF9i (**Fig.30**). In this sample, however, the red underpainting in fresco is even more visible (**Fig.30,b**) with the SEM in BSE, as well as the carbonation layer in-between the paint layers.

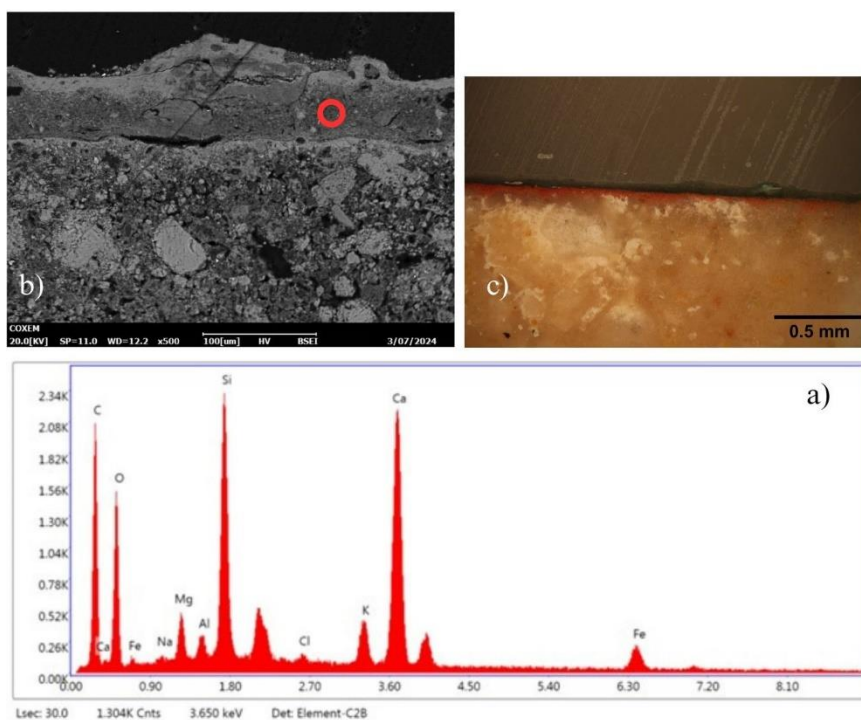


**Figure 30.** a)EDS spectra of the green pictorial layer of sample MF9i. b) SEM image in BSE of the analyzed area and an optical microscope image of the same area.

Therefore, the elemental composition unveiled by the EDS analysis and the observations obtained in the PLM and SEM suggest that the pigment used for the green samples is green earth ( $K[(Al,Fe^{3+}), (Fe^{2+},Mg)](AlSi_3, Si_4)O_{10}(OH)_2$ ), a naturally occurring green pigment celebrated for its artistic applications. Green earth is typically defined as a clay-based pigment containing a chromogenic component within its clay matrix, typically consisting of a hydrated aluminosilicate compound containing Mg, Fe, and K. This pigment can generally be distinguished by its color and chemical and mineralogical composition mainly of aluminosilicate and the presence of Mg (Genestar and Pons, 2005). Specifically, for MF9i (**Fig.30,a**) the substantial presence of O and Si aligns with the occurrence of silicate minerals characteristic of green earth pigments. Additionally, the presence of Fe supports the hypothesis of iron-containing minerals contributing to the green coloration. K is commonly found in green earth pigments and contributes to their mineral composition, while enhancing the stability and coloration of the pigment, influencing its overall appearance and properties. As mentioned before, the relatively high concentration of Ca may be related to the binder or a white pigment. The elevated presence of C can be either attributed to calcium carbonate or to the addition of a carbon black pigment to deepen the hue of the green.

Sample MF5i (third group, blue samples) was examined to verify the use of Egyptian blue for the blue pigments.

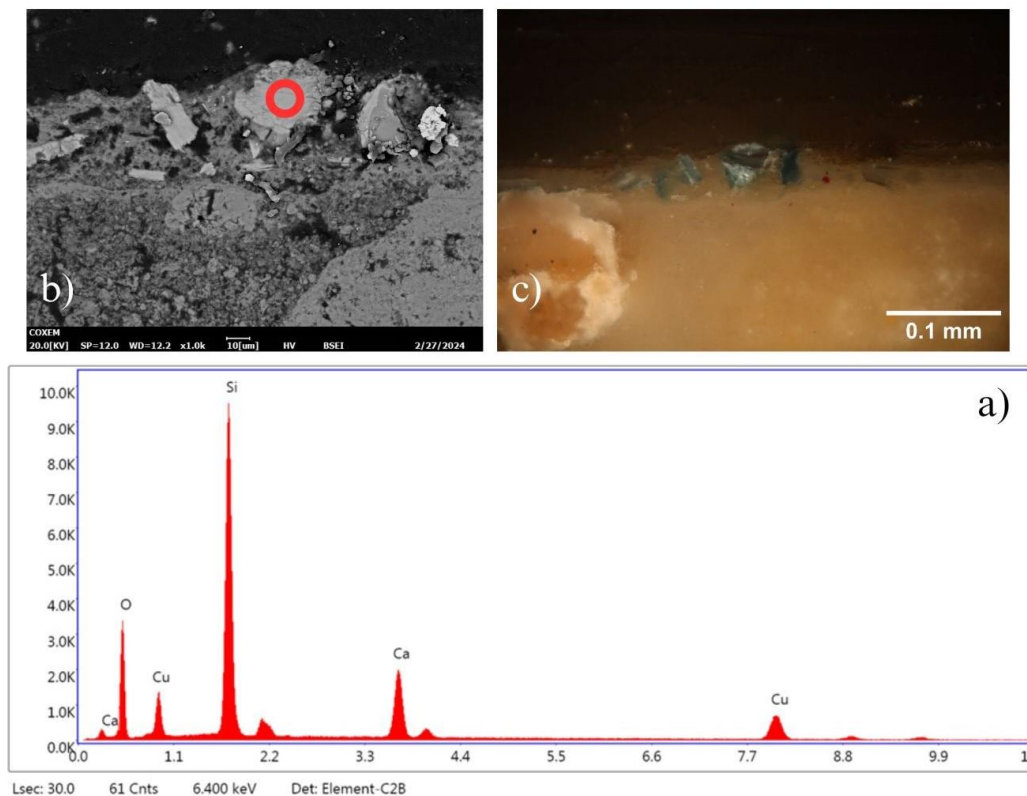


**Figure 31.** a)EDS spectra of the blue lump of pigment of sample MF5i. b) SEM image in BSE of the analyzed lump and an optical microscope image of the respective area.

In this sample (**Fig.31,b**) the carbonation layer between the plaster and paint layer is clearly distinguished. The paint layer is thick and exhibits clear boundaries at the points of contact with the plaster. It has a generally good adhesion to the plaster, observed in the SEM, and it is fairly homogenous with coarse lumps of blue and more rarely red pigments (**Fig.31,c**). The elemental composition of the sample, as indicated by EDS analysis (**Fig.31,a**), consisted with the composition of the expected Egyptian blue pigment detected with micro-Raman spectroscopy, a synthetic pigment composed primarily of Ca copper tetrasilicate ( $\text{CaCuSi}_4\text{O}_{10}$ ). Cu is responsible for the characteristic color of Egyptian blue, with cuprorivaite being the chromophore mineral of Egyptian blue (Aquilina *et al.*, 2012).

For the red samples (fourth group), red ochre was clearly detected with micro-Raman spectroscopy, therefore only MF8 and CF1 were selected to be analyzed with SEM-EDS.

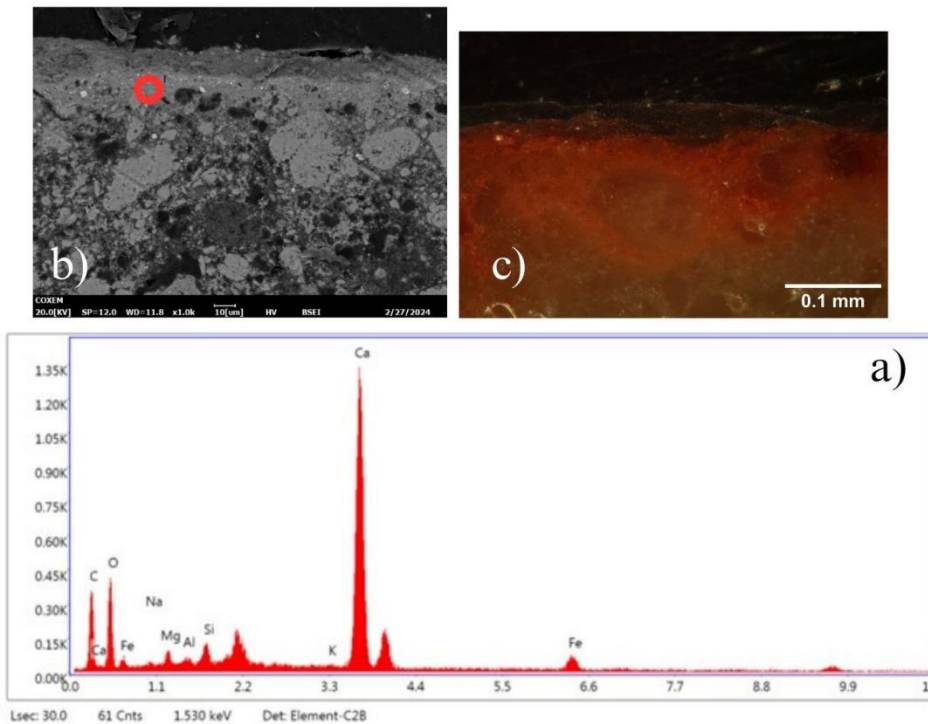


**Figure 32.** a)EDS spectra of the red pictorial layer of sample MF8. b) SEM image in BSE of the analyzed area and an optical microscope image of the same area.

MF8 (**Fig.32,a**) features a red layer applied in fresco, as it is well adhered to the plaster, without any discontinuity, and there is no carbonation layer. In the small green area of the sample that is pictured in **Fig.32,a,b** the green overpainting can also be distinguished. As described for the green pigments, this layer has uniform thickness and grain size and is applied in secco. The microchemical analysis by EDS (**Fig.32,a**) is consistent with the characteristics expected for a red ochre pigment, which consists of hematite usually mixed with different quantities of clay and sand. Fe oxides are key components responsible for the characteristic red hue of ochre pigments, thus the presence of Fe in the EDS spectra (Ashkenazi *et al.*, 2021). The high content of Ca in this sample can be attributed to the fact that this layer is in contact with the plaster and to the binder, likely calcium carbonate. The presence of Pb, detected with micro-Raman is not identified with the present analysis.

CF1 (**Fig.33**) features a distinct microstratigraphy, with a thick preparatory plaster layer clearly visible in the SEM (**Fig.33,b**). This layer has clear and sharp boundaries with the underlying plaster, represented by voids in the SEM image, and with the upper paint layer. The red paint layer has uniform thickness, a fine grain size and is applied in secco, with sporadic coarse-grained lumps of red pigment. As in MF8, the microchemical characteristics (**Fig.33,c**) align with those expected of red ochre pigments. Mn is also detected in this sample, which is typically associated with umbers, pigments related to ochres but differentiated in the fact that they embody a substantial amount of manganese oxides (Mastrotheodoros and Beltsios, 2022). The high presence of C, Si and Ca are related to the binder and the fact that this layer is in contact with the plaster.

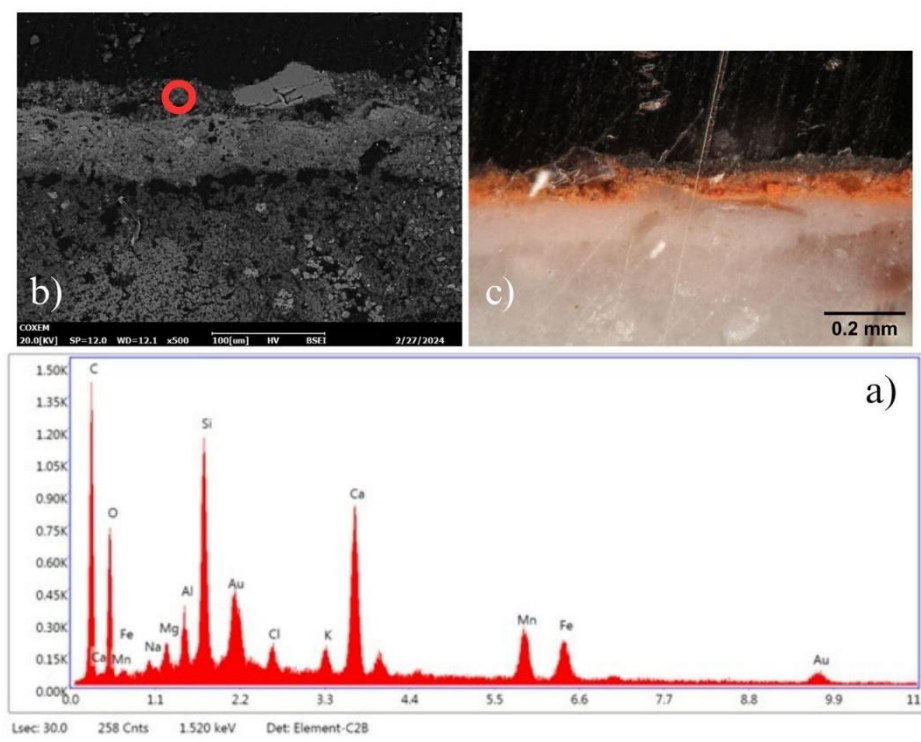


**Figure 33.** a)EDS spectra of the red pictorial layer of sample CF1. b) SEM image in BSE of the analyzed area and an optical microscope image of the same area.

Interestingly, the red overpainting of MF10i (**Fig.34**) was also analyzed with SEM-EDS. Noteworthy is the presence of P in this sample, that could be explained as either due to the mixing of a bone black pigment, or from micro-fragments of bones that had been mixed with the ochre in the production process (Seva Román *et al.*, 2019), that is not, however, consistent with the location of the archaeological site of Motza.

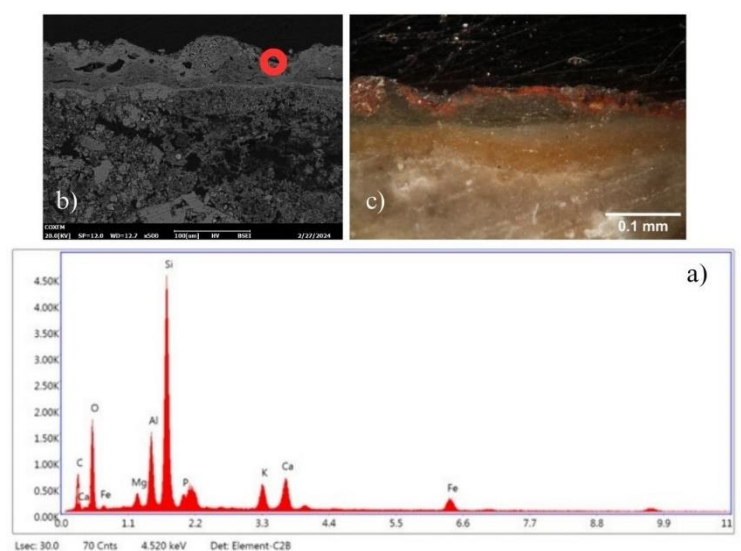


**Figure 34.** a)EDS spectra of the red overpainting layer of sample MF10i. b)SEM image in BSE of the analyzed area and an optical microscope image of the same area.

The overpainting layer presents a non-uniform thickness, with coarse grains of red pigment (**Fig.34,b,c**), and clear boundaries with the green pictorial layer indicating the

use of secco application. A thin carbonation layer is visible between the plaster and the green layer, as observed for all the green pigments, further supporting the use of the secco technique. An interesting feature is the yellow color inside the plaster, appearing thicker, more uniform and with smaller grain size than the rest of the plaster (**Fig.34,b**).

The black sample MF3 (**Fig.35,a**) is characterized by the presence of Ca and P suggesting the presence of hydroxyapatite. The C content is therefore likely attributed to the carbonized remnants of bone tissue, primarily composed of collagen that contributes to the pigment's intense black hue (Tomasini, Siracusano and Maier, 2012). This, along with the C content, can be indicative of the use of a carbon black pigment of animal origin. The use of the fresco technique for the black color is obvious from the SEM image (**Fig.35,b**), as there is no discontinuity between the paint layer and the plaster.

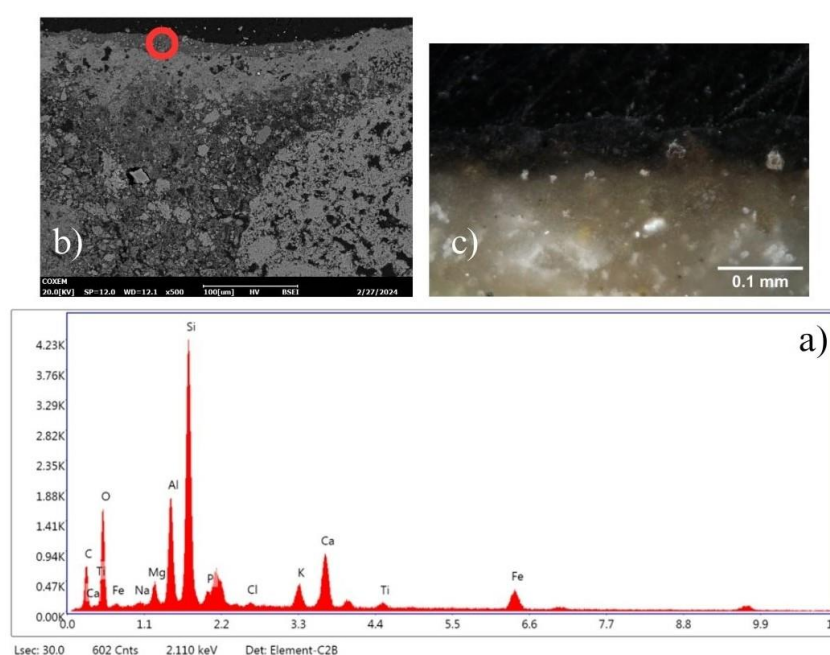


**Figure 35.** a)EDS spectra of the black layer of sample MF3. b) SEM image in BSE of the analyzed area and an optical microscope image of the same area.

The mortars were also analyzed by SEM-EDS. Those from Motza displayed consistent characteristics among themselves, mirroring the uniformity observed in those from Caesarea. Specifically, EDS detected Ca, Si, Mg, Al alongside occasional detection of Na, Cl in varying percentages for the Motza samples (**Fig.36,b**). The main composition of the binder matrix is Ca which shows to us that the binders were made with the use of pure calcic lime. Si and Al correspond to the poorly crystalline phases which develop due to the reaction between the lime and aluminosilicate compounds in a saturated alkaline environment. Mg can be related to dolomitic stones used in the binders as aggregates, and it gives rise to the formation of gel-like M-A-S-H (Mg aluminosilicate hydrates) in the binder matrix (Secco *et al.*, 2022).

Those from Caesarea primarily contain Ca and Si with occasional traces of Al, Mg, Na (**Fig.36,d**). However, although the concentration Ca is significant, as in the samples from Motza, those of Mg and Si are at lower values, suggesting the lack of reactivity

of the components in the mortar, and the binder not having been altered (Secco *et al.*, 2022). The local *kurkar* seems to have been used as an aggregate in those samples, an aeolianite local deposit, which generally presents calcareous stones with gastropods, bivalves, foraminifera, and detritic quartz. This cemented Pleistocene sediment is a beachrock that outcrops along the Mediterranean coastal cliffs of Israel (Vola *et al.*, 2011).

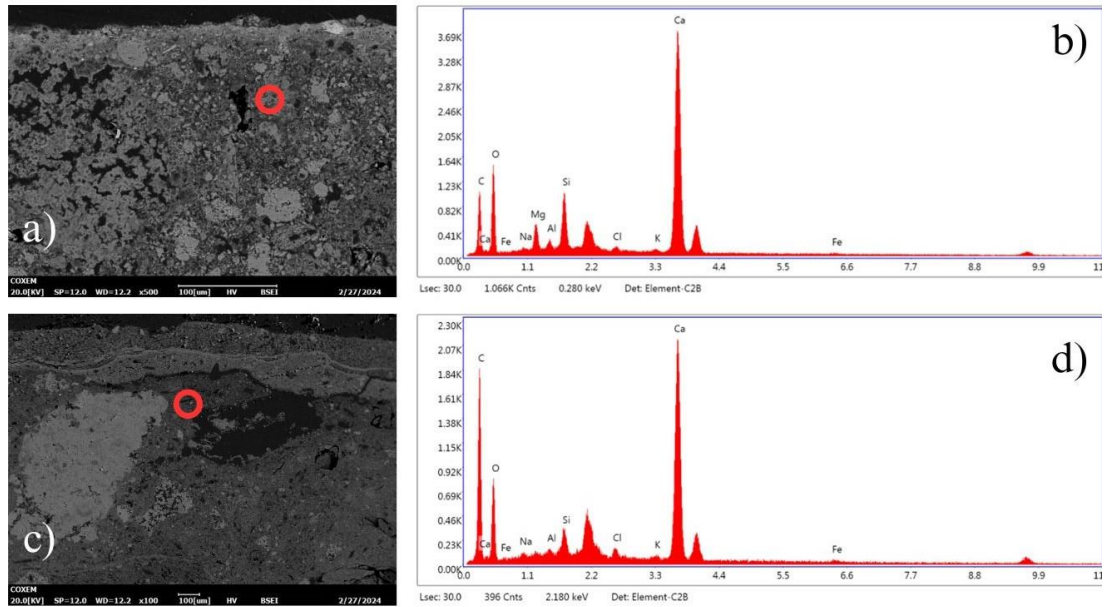


**Figure 36.** a) SEM image in BSE and (b) EDS spectra of the plaster matrix of sample MF8. c) SEM image in BSE and EDS spectra (d) of the plaster of sample CF5i.

The layering of mortars mentioned in previous chapters for the samples from Caesarea is clearly visible in the SEM (**Fig.37**). The lower *kurkar* layer is characterized by its relatively coarser texture and larger aggregate particles, while the preparatory mortar layer exhibits a more homogeneous and fine-grained matrix, typical of lime based mortars (Mohammed Haneefa *et al.*, 2019). The addition of the finer texture mortar provides a smoother and more uniform surface, which is beneficial for the application and adhesion of the subsequent paint layers.

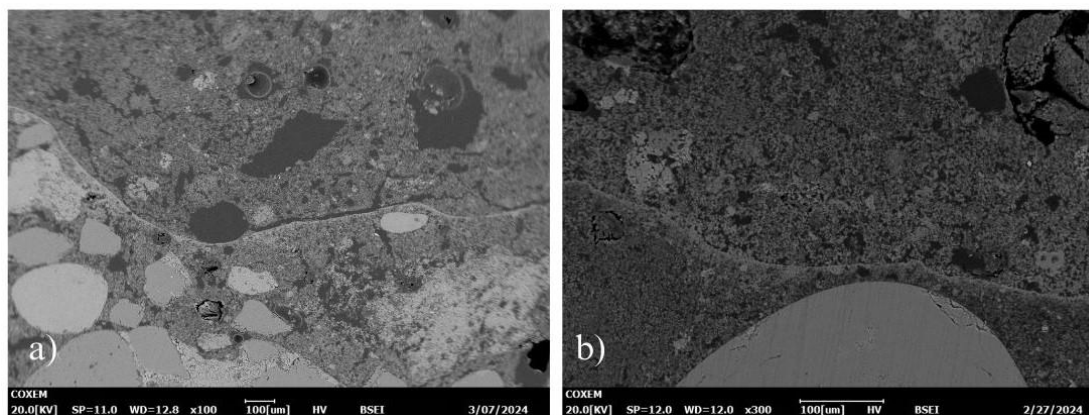


**Figure 37** SEM images in BSE showcasing the layering of mortars in samples from Caesarea.

#### 6.4 X-ray diffraction – X-ray powder diffraction (XRD-XRPD)

As described in chapter 5.6, 8 samples were selected to be analyzed with XRD and 3 with XRPD. In the table below, all phases detected in the XRD/XRPD patterns of each sample are summarized. The samples CF6-M, MF8-M and MF15-M are the ones analyzed with XRPD in a powdered form. Those samples are differently labeled to recognize that only the mortar part of those samples was analyzed.

**Table 4.** Sample names and phases detected with the XRD/XRPD.

	Cal	Qtz	Alb	Hem	Kaol	Mic	Arag	Dol	Goet	Hyx	Cup	Cris	Mucs	Glau	Cel
CF1	x	x	x	x	x										
MF1	x	x			x	x		x	x						
MF3	x	x			x			x		x					
MF4	x	x						x			x	x	x		
MF5	x	x						x			x	x	x		
MF9	x	x												x	x
MF10	x	x						x						x	x
MF15	x	x					x						x		
CF6-M	x	x	x			x	x								
MF8-M	x	x				x	x	x							
MF15-M	x	x					x								

\*Cal: calcite, Qtz: quartz, Alb: albite, Hem: hematite, Kaol: kaolinite, Mic: microcline, Arag: aragonite, Dol: dolomite, Goet: goethite, Hyx: hydroxyapatite, Cup: cuprorivaite, Cris: cristobalite, Musc: muscovite, Glau: glauconite, Cel: celadonite.

Obviously, calcite and quartz were detected in all of the samples. Calcite is generally related to the binder and the mortar. However, it was also detected, along with quartz, through micro-Raman and EDS both as a white pigment and a mortar component.

CF1 is a red sample originating from Caesarea (**Fig.38**). The presence of calcite is widely common in ochre pigments and in binders, the use of which is verified by the detection of hematite, the chromophore mineral of red ochre (Marcaida *et al.*, 2019). Quartz is related to the aggregate fraction and is also usually found among red ochres. Albite is a type of feldspar, specifically a plagioclase feldspar, and it is commonly found in various geological materials, including rocks and sediments. Kaolinite is a clay mineral, known for its resistance to weathering and it's a typical non-chromophore mineral of red ochre deposits.



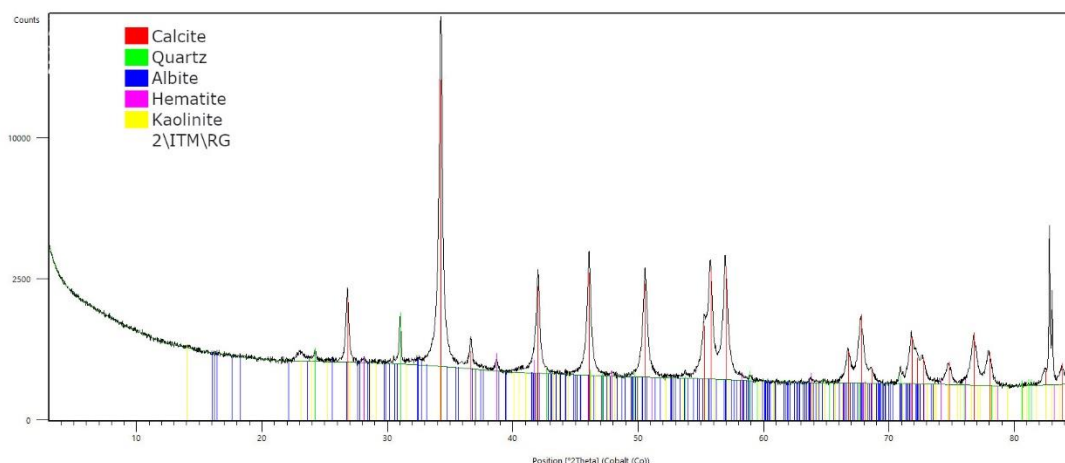


**Figure 38.** XRD pattern of sample CF1

MF1's mustard surface was analyzed with XRD (**Fig.39**). Again, the use of yellow ochre is confirmed by the detection of goethite, the chromophore of yellow ochre. Kaolinite is a clay mineral formed through weathering processes common for yellow ochres, while microcline is a type of feldspar commonly found in igneous rocks (Elias *et al.*, 2006). Finally, dolomite is a carbonate mineral similar to calcite but containing Mg in addition to Ca, with its presence suggesting the use of dolomite-rich rocks in the construction of the wall.

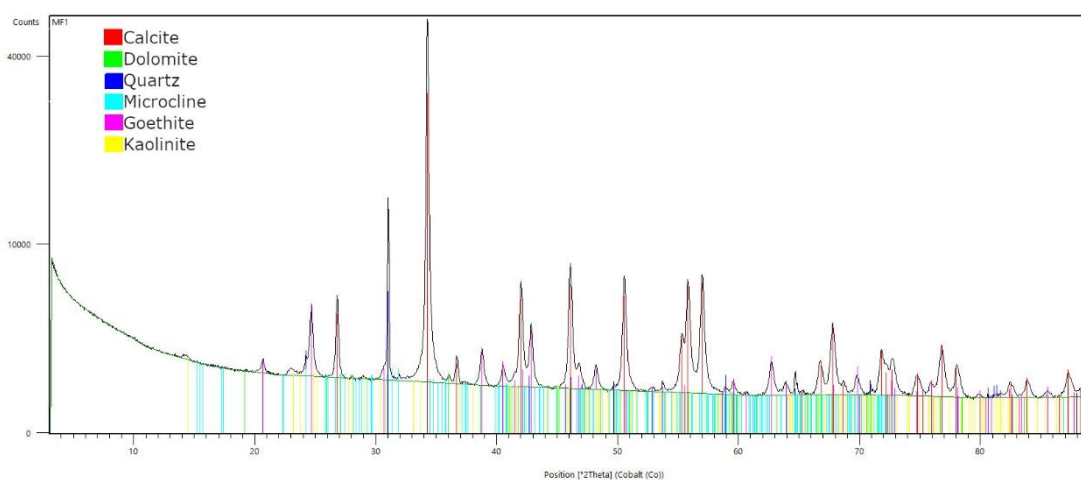


**Figure 39.** XRD pattern of sample MF1.

MF3 is the black colored fragment, which after micro-Raman and EDS analyses the use of bone black was proposed (**Fig.40**). Indeed, hydroxylapatite is the principal component of bone, with bone black being produced by heating animal bones at high temperatures, which decomposes the organic components and leaves behind a residue rich in carbon and mineral components, including hydroxylapatite (Twilley, 2012). Therefore, the use of bone black pigment is confirmed with XRD.

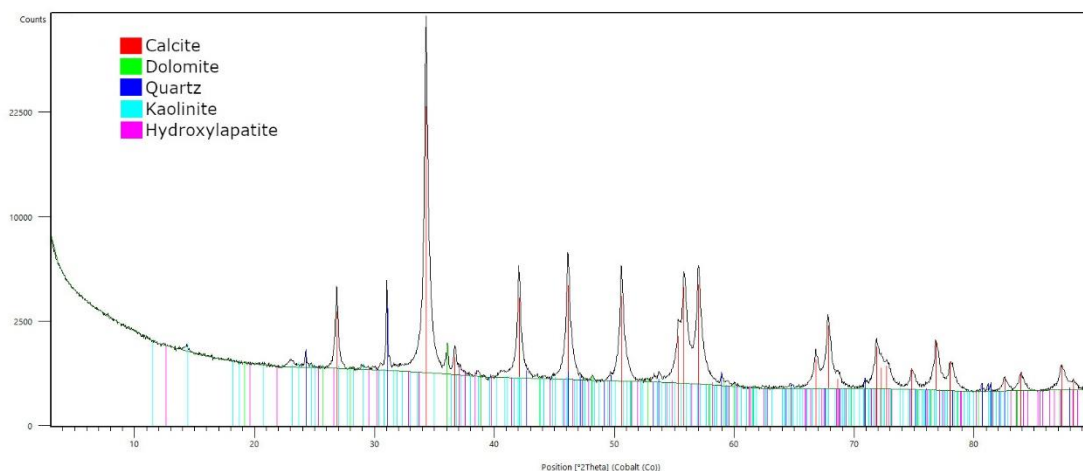


**Figure 40.** XRD pattern of sample MF3.

MF4 and MF5 also presented expected and significant data (**Fig.41**), consistent with Egyptian blue pigment identified with Raman and EDS. The crystalline-phase cuprorivaite provides Egyptian blue with its color. Here, quartz plays a part in the preparation process of the pigment as a non-chromophore mineral, while cristobalite is related to the polymorphic transition of quartz at high temperatures (Chaklader and Roberts, 1961). Muscovite is a type of mica mineral commonly found in metamorphic and igneous rocks, which can be related to aggregate residue in this case.

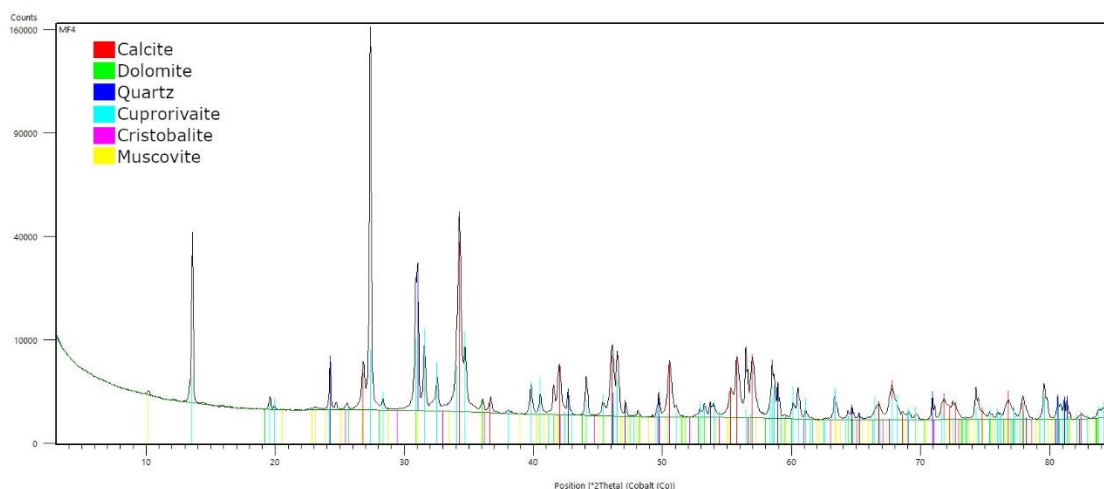


**Figure 41.** XRD pattern of sample MF4.

MF9 exhibits results further supporting those of EDS analysis that green earth was used for the green pigments (**Fig.42**). Specifically, green earth pigments, used since antiquity, primarily consist of micas, namely celadonite and/or glauconite, both of which are phyllosilicates and present in our XRD pattern. These minerals are generated through distinct geological processes (Ospitali *et al.*, 2008; Duran *et al.*, 2011). Similar assessments can be made for MF10 (**Fig.43**), another green sample, however that is deprived of dolomite.

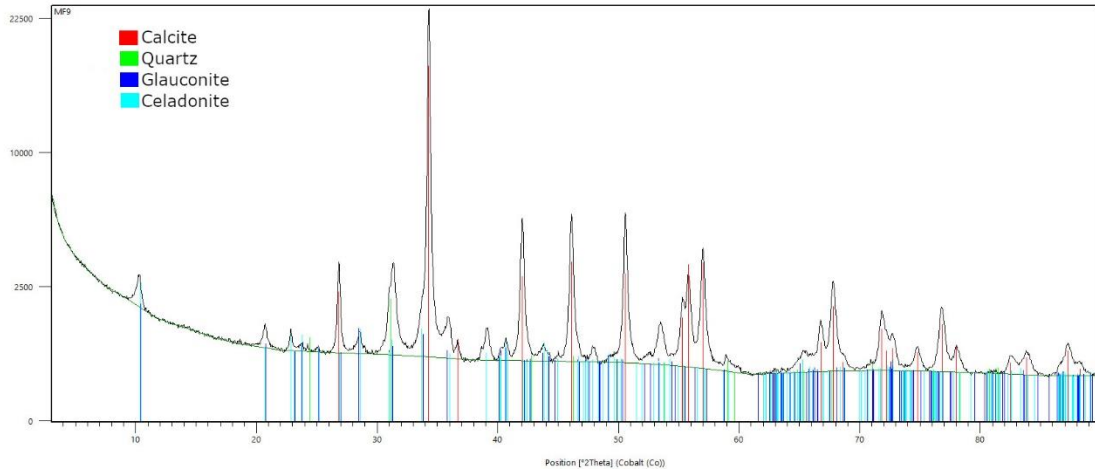


**Figure 42.** XRD pattern of sample MF9.

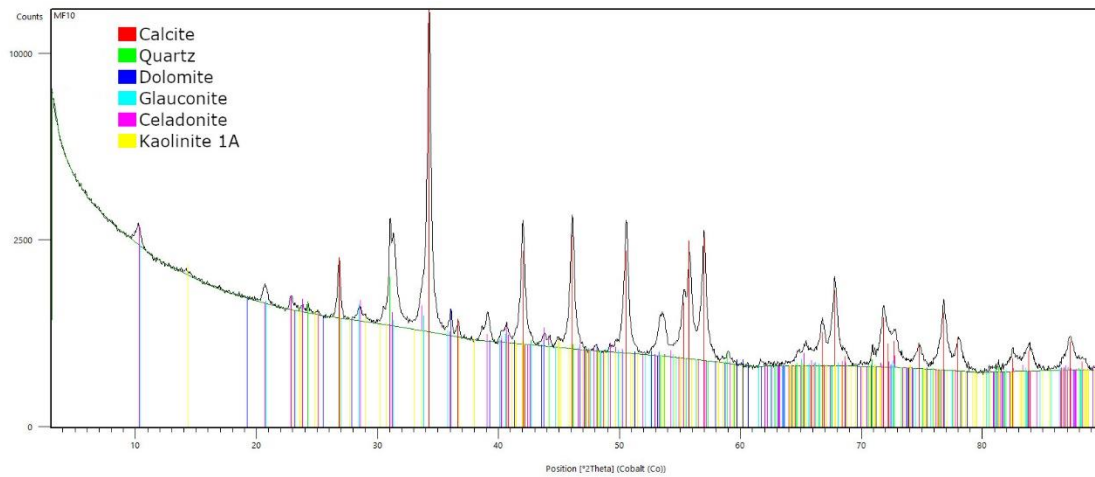


**Figure 43.** XRD pattern of sample MF10.

MF15, a red sample, features results that match those from previous analyses that red ochre was employed in the red pigments (**Fig.44**). The presence of aragonite, a polymorph of calcium carbonate, could be potentially related to the addition of a white pigment or to the substrate, as it is also detected in the powdered samples (Edwards *et al.*, 2001).

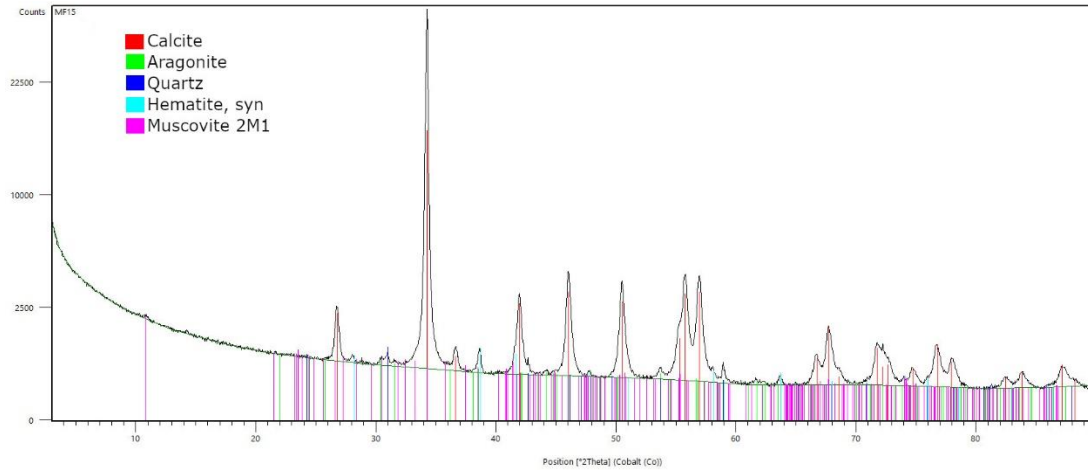


**Figure 44.** XRD pattern of sample MF15.

In CF6-M, the sole sample from Caesarea, calcite is related to the binder and aggregate, which seems to be the local *kurkar* with residue of feldspars, thus the presence of albite and microcline. Aragonite, as already mentioned, is one of the mineralogical forms of Ca carbonate, of biogenic origin (shells, coral, pearls). When found in the mortar, it is ascribed to the aggregate fraction, as the production of lime, also from the calcination of shells, facilitates the formation of calcite. The most common source of aragonite are mollusk shells and endoskeleton corals (Rampazzi *et al.*, 2021). Therefore, the mortar consists of lime binder, indicated additionally by the presence of calcite, mixed with sandstone, the *kurkar*.

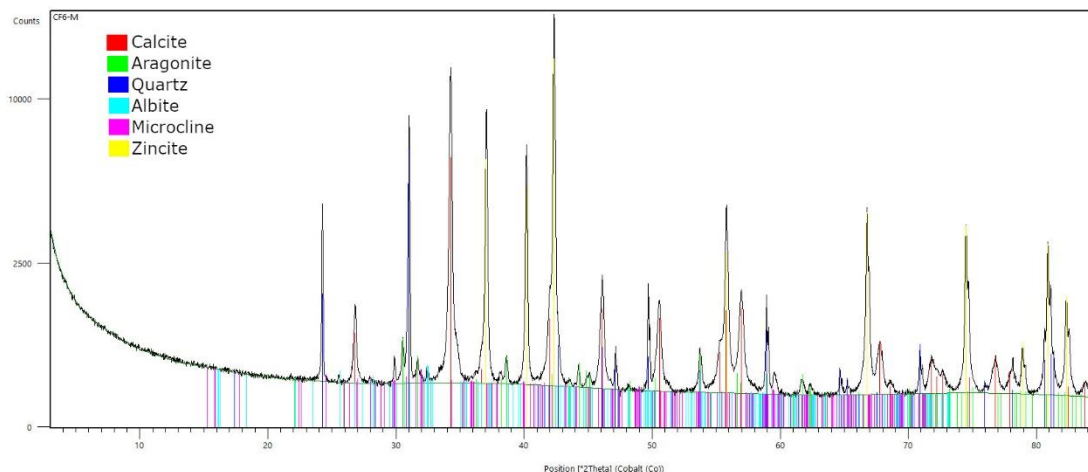


**Figure 45.** XRPD pattern of sample CF6-M.

MF8-M (**Fig.46**) and MF15-M (**Fig.47**) both display same characteristics, however in MF8 dolomite and microcline are also identified. There is a high amount of aragonite in both samples that could be attributed either to the carbonation of lime and pozzolanic reaction, or to the aggregate consisting of shell components, a possibility that was not, however, visible in the optical microscope or SEM. The non-uniform presence of

dolomite raises questions on whether dolomitic rocks were used in the construction of the wall, although there are case studies that support this case (Maor *et al.*, 2023). To gain deeper clarity, employing alternative methodologies such as Fourier-transform infrared spectroscopy (FTIR) or X-ray powder diffraction (XRPD) on the binder fraction could offer more comprehensive insights into the composition and origins of the material.

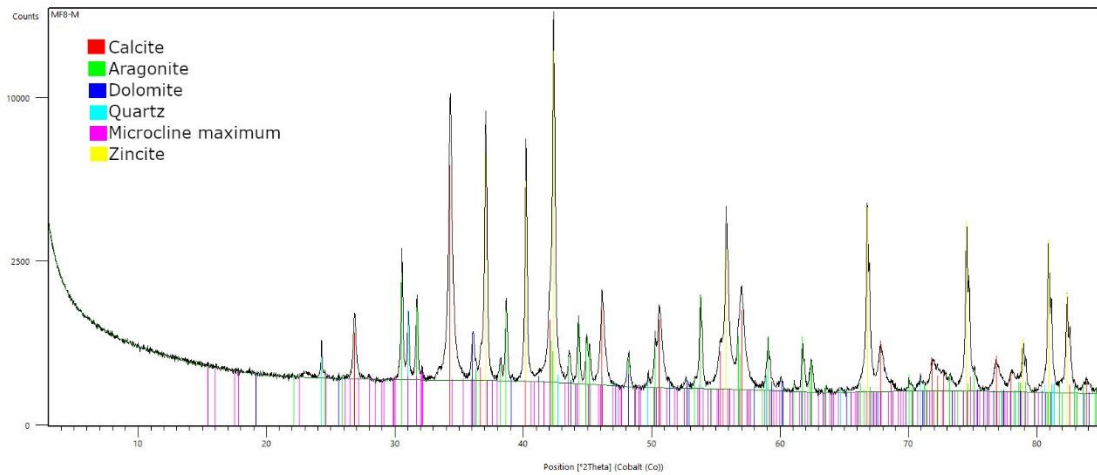


Figure 46. XRPD pattern of sample MF8-M.

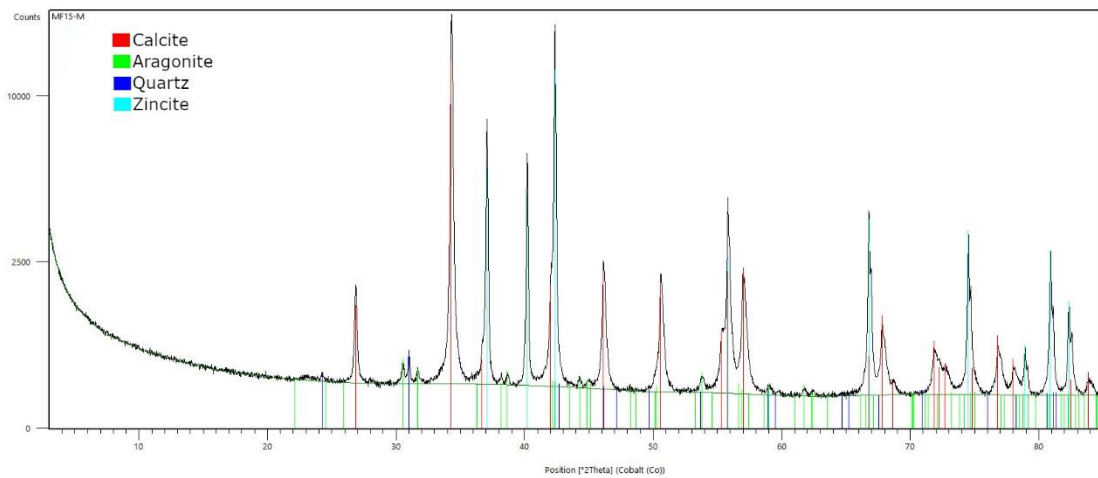


Figure 47. XRPD pattern of sample MF15-M.

## 7. Conclusions

This research focused on identifying the techniques and materials used in creating mural paintings in Motza and Caesarea, employing a multidisciplinary approach that included Optical Microscopy, micro-Raman Spectroscopy, Scanning Electron Microscopy, and X-Ray Diffraction/X-ray Powder Diffraction. The findings provide significant insights into the artistic practices and technological knowledge of the ancient civilizations that inhabited these sites.

The chemical and mineralogical examination of the cross-section samples revealed the use of various pigments, such as yellow and red ochre, Egyptian blue, green earth and carbon black. Notably, the *secco* technique, which involves applying pigments to dry plaster, was predominantly used, along with fresco and lime painting. The use of various techniques highlights the advanced understanding of materials and chemical processes by Roman artists.

The mineralogical and chemical analyses on the mortars demonstrated different aspects of mortar technology. Mortars from Motza consist mostly of lime and they exhibit characteristics related to pozzolanic reactions. These reactions occur when lime interacts with siliceous or aluminous materials, creating compounds that enhance the mortar's strength and durability. The use of lime and pozzolanic materials indicates a sophisticated knowledge of construction materials, ensuring the longevity and stability of the murals. For those from Caesarea mostly lime and the local *kurkar* were used to create the ideal substrate for the painting application.

The detailed characterization of the mural paintings' materials and techniques provides valuable information not only for conservation efforts but for enhancing the knowledge on the archaeological sites of Motza and Caesarea. Further investigation into the provenance of the pigments and raw materials could help in building a more comprehensive understanding. Specifically, the presence of dolomite in the mortars from Motza should be further investigated, as well as the presence of minerals such as Mn found in some of the red pigments.

In conclusion, this research on the mural paintings from Motza and Caesarea Maritima offers a unique window into the artistic and cultural practices of the Roman period in the Eastern Mediterranean.

## 8. Bibliography

- Ad, U., Bar-Nathan, R. and Taxel, I. (2022) “‘Ad, U., Bar-Nathan, R. And Taxel, I. 2022. The Roman Veterans” Settlement at Moza c. AD 70–130. In: Atrash, A., Overman, A. and Gendelman, P. (eds.). *Cities, Monuments and Objects in the Roman and Byzantine Levant. Studies in Honour of Gabi Mazor*. Oxford. Pp. 148-156.’, pp. 148–156.
- Aquila, E. *et al.* (2012) ‘Spectroscopic analyses of Hellenistic painted plasters from 2nd century B.C., Sicily (South Italy)’, *Journal of Cultural Heritage*, 13(2), pp. 229–233. Available at: <https://doi.org/10.1016/j.culher.2011.09.006>.
- Artioli, G. (2010) *Scientific Methods and Cultural Heritage: An introduction to the application of materials science to archaeometry and conservation science*. Oxford University Press. Available at: <https://doi.org/10.1093/acprof:oso/9780199548262.001.0001>.
- Ashkenazi, D. *et al.* (2021) ‘Chemical Composition and Microstructure Analysis of Plaster and Pigments Retrieved from a Decorated House Wall at Seleucid Tell Iztabba (Nysa-Scythopolis, Beth She’an, Israel)’, *Mediterranean Archaeology and Archaeometry*, 21, pp. 89–122. Available at: <https://doi.org/10.5281/zenodo.5598239>.
- Baraldi, P. *et al.* (2001) ‘Study of the vibrational spectrum of cuprorivaite’, *Annali di chimica*, 91, pp. 679–92.
- Chaklader, A.C.D. and Roberts, A.L. (1961) ‘Transformation of Quartz to Cristobalite’, *Journal of the American Ceramic Society*, 44(1), pp. 35–41. Available at: <https://doi.org/10.1111/j.1151-2916.1961.tb15344.x>.
- Cornale, P. *et al.* (2005) ‘Affresco e mezzofresco: studio sperimentale e procedure analitiche per la caratterizzazione delle tecniche pittoriche’, in *Sulle Pitture Murali. Riflessioni, conoscenza, interventi*. (XXI), pp. 687–696. Available at: <https://www.research.unipd.it/handle/11577/2433566> (Accessed: 19 March 2024).
- Corso, G. *et al.* (2012) ‘Polar and non-polar organic binder characterization in Pompeian wall paintings: comparison to a simulated painting mimicking an “a secco” technique’, *Analytical and Bioanalytical Chemistry*, 402(9), pp. 3011–3016. Available at: <https://doi.org/10.1007/s00216-012-5746-8>.
- Cosano, D. *et al.* (2019) ‘Identification of pigments in the Annunciation sculptural group (Cordoba, Spain) by micro-Raman spectroscopy’, *Spectrochimica Acta Part A: Molecular and Biomolecular Spectroscopy*, 214, pp. 139–145. Available at: <https://doi.org/10.1016/j.saa.2019.02.019>.
- Donnelly, F. *et al.* (2017) ‘Synthesis of CaCO<sub>3</sub> nano- and micro- particles by dry ice carbonation’, *Chem. Commun.*, 53. Available at: <https://doi.org/10.1039/C7CC01420A>.
- Duran, A. *et al.* (2011) ‘Analytical study of Roman and Arabic wall paintings in the *Patio De Banderas* of Reales Alcazares’ Palace using non-destructive XRD/XRF and complementary techniques’, *Journal of Archaeological Science*, 38(9), pp. 2366–2377. Available at: <https://doi.org/10.1016/j.jas.2011.04.021>.

- Edwards, H. *et al.* (2001) 'Mediaeval Pigments in the Monastery of San Baudelio, Spain: A Raman Spectroscopic Analysis', *Applied Spectroscopy - APPL SPECTROSC*, 55, pp. 71–76. Available at: <https://doi.org/10.1366/0003702011951272>.
- Elias, M. *et al.* (2006) 'The colour of ochres explained by their composition', *Materials Science and Engineering: B*, 127(1), pp. 70–80. Available at: <https://doi.org/10.1016/j.mseb.2005.09.061>.
- Fuhrmann-Naaman, Y. (2017) 'Ancient Caesarea, Conservation and Development of a Heritage Site', *Ancient Caesarea, Conservation and Development of a Heritage Site* [Preprint]. Available at: [https://www.academia.edu/78627973/Ancient\\_Caesarea\\_Conservation\\_and\\_Development\\_of\\_a\\_Heritage\\_Site](https://www.academia.edu/78627973/Ancient_Caesarea_Conservation_and_Development_of_a_Heritage_Site) (Accessed: 20 March 2024).
- Gendelman, P. and Gersht, R. (1997) 'The House of Dioscuri at Caesarea', *Qadmoniot*, 153, pp. 33–42.
- Genestar, C. and Pons, C. (2005) 'Earth pigments in painting: characterisation and differentiation by means of FTIR spectroscopy and SEM-EDS microanalysis', *Analytical and Bioanalytical Chemistry*, 382(2), pp. 269–274. Available at: <https://doi.org/10.1007/s00216-005-3085-8>.
- Germinario, L. *et al.* (2023) 'Petrographic and Chemical Characterization of the Frescoes by Saturnino Gatti (Central Italy, 15th Century)', *Applied Sciences*, 13(12), p. 7223. Available at: <https://doi.org/10.3390/app13127223>.
- Greenhut, Z. *et al.* (2009) *Salvage Excavations at Tel Moza: the Bronze and Iron Age Settlements and Later Occupations*. Israel Antiquities Authority / העתיקות רשות. Available at: <https://doi.org/10.2307/j.ctt1fzhd2b>.
- Gutman, M. *et al.* (2016) 'Wall Paintings from the Roman Emona (Ljubljana, Slovenia): Characterization of Mortar Layers and Pigments', *Archaeometry*, 58(2), pp. 297–314. Available at: <https://doi.org/10.1111/arcm.12167>.
- Hallett, C.H. (2015) 'Defining Roman Art', in *A Companion to Roman Art*. John Wiley & Sons, Ltd, pp. 9–33. Available at: <https://doi.org/10.1002/9781118886205.ch1>.
- Hanesch, M. (2009) 'Raman spectroscopy of iron oxides and (oxy)hydroxides at low laser power and possible applications in environmental magnetic studies', *Geophysical Journal International*, 177(3), pp. 941–948. Available at: <https://doi.org/10.1111/j.1365-246X.2009.04122.x>.
- Hernanz, A. *et al.* (2008) 'Micro-Raman spectroscopic investigation of external wall paintings from St. Dumitru's Church, Suceava, Romania', *Analytical and Bioanalytical Chemistry*, 392(1), pp. 263–268. Available at: <https://doi.org/10.1007/s00216-008-2262-y>.
- Holum, K.G., Stabler, J.A. and Reinhardt, E.G. (2008) *Caesarea Reports and Studies*. Illustrated edition. Oxford: British Archaeological Reports.



Jorge-Villar, S.E. and Edwards, H.G.M. (2021) ‘Green and blue pigments in Roman wall paintings: A challenge for Raman spectroscopy’, *Journal of Raman Spectroscopy*, 52(12), pp. 2190–2203. Available at: <https://doi.org/10.1002/jrs.6118>.

Josephus (1928) *The Jewish War, Volume III*. Translated by H.St.J. Thackeray. Cambridge, MA: Harvard University Press (Loeb Classical Library (LCL) 210). Available at: <https://www.loebclassics.com/view/LCL210/1928/volume.xml> (Accessed: 19 March 2024).

Kisilevitz, S. and Lipschits, O. (2019) ‘Tel Moza.: An Economic and Cultic Center from the Iron Age II (First Temple Period)’, in, pp. 295–312. Available at: <https://doi.org/10.2307/j.ctv1b9f5bh.14>.

Maor, Y. *et al.* (2023) ‘Dolomite in archaeological plaster: An FTIR study of the plaster floors at Neolithic Motza, Israel’, *Journal of Archaeological Science: Reports*, 48, p. 103862. Available at: <https://doi.org/10.1016/j.jasrep.2023.103862>.

Marcaida, I. *et al.* (2019) ‘Raman microscopy as a tool to discriminate mineral phases of volcanic origin and contaminations on red and yellow ochre raw pigments from Pompeii’, *Journal of Raman Spectroscopy*, 50(2), pp. 143–149. Available at: <https://doi.org/10.1002/jrs.5414>.

Mastrotheodoros, G.P. and Beltsios, K.G. (2022) ‘Pigments—Iron-based red, yellow, and brown ochres’, *Archaeological and Anthropological Sciences*, 14(2), p. 35. Available at: <https://doi.org/10.1007/s12520-021-01482-2>.

Mohammed Haneefa, K. *et al.* (2019) ‘Microstructure and geochemistry of lime plaster mortar from a heritage structure’, *Construction and Building Materials*, 225, pp. 538–554. Available at: <https://doi.org/10.1016/j.conbuildmat.2019.07.159>.

bar-nathan, rachel, Di Segni, L. and Taxel, I. (2020) ‘Bar-Nathan, R., Zilberbod, I., Landes-Nagar, A., Di Segni, L. and Taxel, I. 2020. Moza in the First Centuries CE: On the Identification and Nature of Roman Colonia.’

Needham, A. *et al.* (2018) ‘The application of micro-Raman for the analysis of ochre artefacts from Mesolithic palaeo-lake Flixton’, *Journal of Archaeological Science: Reports*, 17, pp. 650–656. Available at: <https://doi.org/10.1016/j.jasrep.2017.12.002>.

Ospitali, F. *et al.* (2008) ‘“Green earths”: vibrational and elemental characterization of glauconites, celadonites and historical pigments’, *Journal of Raman Spectroscopy*, 39(8), pp. 1066–1073. Available at: <https://doi.org/10.1002/jrs.1983>.

Perez-Rodriguez, J.L. *et al.* (2014) ‘Wall paintings studied using Raman spectroscopy: A comparative study between various assays of cross sections and external layers’, *Spectrochimica Acta Part A: Molecular and Biomolecular Spectroscopy*, 120, pp. 602–609. Available at: <https://doi.org/10.1016/j.saa.2013.10.052>.

Piovesan, R. *et al.* (2011) ‘The Temple of Venus (Pompeii): a study of the pigments and painting techniques’, *Journal of Archaeological Science*, 38(10), pp. 2633–2643. Available at: <https://doi.org/10.1016/j.jas.2011.05.021>.

- Piovesan, R. *et al.* (2012) ‘Fresco and Lime-Paint: An Experimental Study and Objective Criteria for Distinguishing Between These Painting Techniques’, *Archaeometry*, 54(4), pp. 723–736. Available at: <https://doi.org/10.1111/j.1475-4754.2011.00647.x>.
- Pliny, G. (1952) *Natural History*. Translated by H. Rackham. Cambridge, MA: Harvard University Press (Loeb Classical Library).
- Portella, I.D. (2007) *Subterranean Rome. Ediz. illustrata*. Illustrated edizione. Translated by R. Pierce. San Giovanni Lupatoto: Arsenale.
- Pronti, L. *et al.* (2020) ‘Advanced methods for the analysis of Roman wall paintings: elemental and molecular detection by means of synchrotron FT-IR and SEM micro-imaging spectroscopy’, *Rendiconti Lincei. Scienze Fisiche e Naturali*, 31(2), pp. 485–493. Available at: <https://doi.org/10.1007/s12210-020-00888-9>.
- Rabbān, A. and Holum, K.G. (1996) *Caesarea Maritima: A Retrospective After Two Millennia*. BRILL.
- Rampazzi, L. *et al.* (2021) ‘Unexpected Findings in 16th Century Wall Paintings: Identification of Aragonite and Unusual Pigments’, *Heritage*, 4(3), pp. 2431–2448. Available at: <https://doi.org/10.3390/heritage4030137>.
- Regazzoni, L. *et al.* (2018) ‘Microscopic Analysis of Wall Painting Techniques: Laboratory Replicas and Romanesque Case Studies in Southern Switzerland’, *Studies in Conservation*, 63(6), pp. 326–341. Available at: <https://doi.org/10.1080/00393630.2017.1422891>.
- Secco, M. *et al.* (2020) ‘Technological transfers in the Mediterranean on the verge of Romanization: Insights from the waterproofing renders of Nora (Sardinia, Italy)’, *Journal of Cultural Heritage*, 44, pp. 63–82. Available at: <https://doi.org/10.1016/j.culher.2020.01.010>.
- Secco, M. *et al.* (2021) ‘Ochre-Based Pigments in the Tablinum of the House of the Bicentenary (Herculaneum, Italy) between Decorative Technology and Natural Disasters’, *Minerals*, 11(1), p. 67. Available at: <https://doi.org/10.3390/min11010067>.
- Secco, M. *et al.* (2022) ‘Cementation processes of Roman pozzolanic binders from Caesarea Maritima (Israel)’, *Construction and Building Materials*, 355, p. 129128. Available at: <https://doi.org/10.1016/j.conbuildmat.2022.129128>.
- Seva Román, R. *et al.* (2019) ‘Sources of the ochres associated with the Lower Magdalenian “Red Lady” human burial and rock art in El Mirón Cave (Cantabria, Spain)’, *Journal of Archaeological Science: Reports*, 23, pp. 265–280. Available at: <https://doi.org/10.1016/j.jasrep.2018.10.024>.
- Sharma, S. *et al.* (2006) ‘Remote Raman Spectroscopy of Various Mixed and Composite Mineral Phases at 7.2 m Distance’.
- Siddall, R. (2006) ‘Not a day without a line drawn: Pigments and painting techniques of Roman Artists’, *infocus Magazine*, p. 18.

Tomasini, E., Siracusano, G. and Maier, M.S. (2012) ‘Spectroscopic, morphological and chemical characterization of historic pigments based on carbon. Paths for the identification of an artistic pigment’, *Microchemical Journal*, 102, pp. 28–37. Available at: <https://doi.org/10.1016/j.microc.2011.11.005>.

Twilley, J. (2012) ‘13. Pigment Analyses for the Grave Stelai and Architectural Fragments from Chersonesos’, in *13. Pigment Analyses for the Grave Stelai and Architectural Fragments from Chersonesos*. University of Texas Press, pp. 455–462. Available at: <https://doi.org/10.7560/723122-017>.

Uvarov, V., Popov, I. and Rozenberg, S. (2015) ‘X-ray Diffraction and SEM Investigation of Wall Paintings Found in the Roman Temple Complex at Horvat Omrit, Israel’, *Archaeometry*, 57(5), pp. 773–787. Available at: <https://doi.org/10.1111/arc.12124>.

Vančo, L. *et al.* (2013) ‘Examining the ground layer of St. Anthony from Padua 19th century oil painting by Raman spectroscopy, scanning electron microscopy and X-ray diffraction’, *Applied Surface Science*, 264, pp. 692–698. Available at: <https://doi.org/10.1016/j.apsusc.2012.10.099>.

Vitruvius, P. (1999) *The Ten Books on Architecture*. Translated by I.D. Rowland. Cambridge, UK: Cambridge University Press.

Vola, G. *et al.* (2011) ‘Chemical, mineralogical and petrographic characterization of Roman ancient hydraulic concretes cores from Santa Liberata, Italy, and Caesarea Palestinae, Israel’, *Periodico di Mineralogia*, 80, pp. 317–338. Available at: <https://doi.org/10.2451/2011PM0023>.